
AFRL-RY-WP-TR-2014-0209

# SIGNAL-TO-NOISE RATIO EFFECTS ON APERTURE SYNTHESIS FOR DIGITAL HOLOGRAPHIC LADAR

**Maureen Crotty, Edward Watson, and David Rabb**

**Ladar Technology Branch**
**Multispectral Sensing & Detection Division**

**AUGUST 2014**
**Interim Report**



**AIR FORCE RESEARCH LABORATORY**
**SENSORS DIRECTORATE**
**WRIGHT-PATTERSON AIR FORCE BASE, OH 45433-7320**
**AIR FORCE MATERIEL COMMAND**
**UNITED STATES AIR FORCE**

# NOTICE AND SIGNATURE PAGE

Using Government drawings, specifications, or other data included in this document for any purpose other than Government procurement does not in any way obligate the U.S. Government. The fact that the Government formulated or supplied the drawings, specifications, or other data does not license the holder or any other person or corporation; or convey any rights or permission to manufacture, use, or sell any patented invention that may relate to them.

This report was cleared for public release by the USAF 88th Air Base Wing (88 ABW) Public Affairs Office (PAO) and is available to the general public, including foreign nationals. Copies may be obtained from the Defense Technical Information Center (DTIC) (http://www.dtic.mil).

AFRL-RY-WP-TR-2014-0209 HAS BEEN REVIEWED AND IS APPROVED FOR PUBLICATION IN ACCORDANCE WITH ASSIGNED DISTRIBUTION STATEMENT.

*//Signature//

DAVID J. RABB, Project Engineer
LADAR Technology Branch
Multispectral Sensing & Detection Division

//Signature//

BRIAN D. EWERT, Chief
LADAR Technology Branch
Multispectral Sensing & Detection Division

//Signature//

TRACY W. JOHNSTON, Chief
Multispectral Sensing & Detection Division
Sensors Directorate

This report is published in the interest of scientific and technical information exchange, and its publication does not constitute the Government's approval or disapproval of its ideas or findings.

*Disseminated copies will show "//Signature//" stamped or typed above the signature blocks.

# REPORT DOCUMENTATION PAGE

*Form Approved*
*OMB No. 0704-0188*



| 1. REPORT DATE *(DD-MM-YY)* | 2. REPORT TYPE | 3. DATES COVERED *(From - To)* |
|---|---|---|
| August 2014 | Interim | 1 January 2011 – 31 October 2012 |

**4. TITLE AND SUBTITLE**
SIGNAL-TO-NOISE RATIO EFFECTS ON APERTURE SYNTHESIS FOR DIGITAL HOLOGRAPHIC LADAR

**5a. CONTRACT NUMBER**
In-House

**5b. GRANT NUMBER**

**5c. PROGRAM ELEMENT NUMBER**
62204F

**6. AUTHOR(S)**
Maureen Crotty, Edward Watson, and David Rabb

**5d. PROJECT NUMBER**
2003

**5e. TASK NUMBER**
11

**5f. WORK UNIT NUMBER**
Y023

**7. PERFORMING ORGANIZATION NAME(S) AND ADDRESS(ES)**
Ladar Technology Branch
Multispectral Sensing & Detection Division
Air Force Research Laboratory, Sensors Directorate
Wright-Patterson Air Force Base, OH 45433-7320
Air Force Materiel Command, United States Air Force

**8. PERFORMING ORGANIZATION REPORT NUMBER**
AFRL-RY-WP-TR-2014-0209

**9. SPONSORING/MONITORING AGENCY NAME(S) AND ADDRESS(ES)**
Air Force Research Laboratory
Sensors Directorate
Wright-Patterson Air Force Base, OH 45433-7320
Air Force Materiel Command
United States Air Force

**10. SPONSORING/MONITORING AGENCY ACRONYM(S)**
AFRL/RYMM

**11. SPONSORING/MONITORING AGENCY REPORT NUMBER(S)**
AFRL-RY-WP-TR-2014-0209

**12. DISTRIBUTION/AVAILABILITY STATEMENT**
Approved for public release; distribution unlimited.

**13. SUPPLEMENTARY NOTES**
PAO Case Number 88ABW-2012-0792, Clearance Date 29 NOV 2012. Report contains color.

**14. ABSTRACT**

The cross-range resolution of a ladar system can be improved by synthesizing a large aperture from multiple smaller sub-apertures. This aperture synthesis requires a coherent combination of the sub-apertures; that is, the sub-apertures must be properly phased and placed with respect to each other. One method that has been demonstrated in the literature to coherently combine the sub-apertures is to cross-correlate the speckle patterns imaged in overlapping regions. This work investigates the effect of low SNR on an efficient speckle cross-correlation registration algorithm with sub-pixel accuracy. Specifically, the algorithms ability to estimate relative piston and tilt errors between sub-apertures at low signal levels is modeled and measured. The effects of these errors on image quality are examined using the MTF as a metric. The results demonstrate that in the shot noise limit, with signal levels as low as about 0.02 signal photoelectrons per pixel in a typical CCD, the registration algorithm estimates relative piston and tilt accurately to within 0.1 radians of true piston and 0.1 waves of true tilt. If the sub-apertures are not accurately aligned in the synthetic aperture, then the image quality degrades as the number of sub-apertures increases.

**15. SUBJECT TERMS**
digital holography, laser, active imaging, remote sensing, laser imaging

| 16. SECURITY CLASSIFICATION OF: | | | 17. LIMITATION OF ABSTRACT: | 18. NUMBER OF PAGES | 19a. NAME OF RESPONSIBLE PERSON (Monitor) |
|---|---|---|---|---|---|
| a. REPORT | b. ABSTRACT | c. THIS PAGE | | | David Rabb |
| Unclassified | Unclassified | Unclassified | SAR | 80 | 19b. TELEPHONE NUMBER *(Include Area Code)* N/A |

# TABLE OF CONTENTS

**Section** **Page**

# LIST OF FIGURES

**Figure** **Page**

**Figure** **Page**

# LIST OF TABLES

**Table** **Page**

# 1 INTRODUCTION

The resolution of an imaging system can be improved by using a smaller wavelength or a larger aperture. Therefore optical wavelengths can be used to increase image resolution more so than radio wavelengths. However optical wavelengths do not propagate through the atmosphere as easily as radio waves. Also due to the high frequency of these waves it is impossible to directly measure the optical signal fields. Below, multiple techniques will be explained to overcome these problems. The next step in designing these systems is to make them cheaper and more efficient. This work specifically investigates low signal situations and how they affect the image quality of synthetic aperture imaging systems.

## 1.1 Motivation

Laser imaging systems come in a few different forms: mono-static or bi-static, coherent or direct detection, heterodyne or homodyne, scanning or flood illuminating, etc. Coherent laser radar (ladar) systems use a laser to illuminate a target and then record the signal that comes back to a receiver mixed with a local oscillator (LO). By mixing the signal with an LO, the signal field can be digitally extracted in post processing. The resolution of ladar systems is limited by the size of the diffraction limit of the receive aperture. In order to overcome this limitation multiple apertures can be used to view the target from different angles or positions and then be combined into a larger synthetic aperture. The resolution increases as a function of the synthetic aperture diameter.

The sub-apertures can be captured and synthesized in many different ways. For instance multiple apertures in a single aperture array can be used to make a larger effective aperture [1-6]. These sparse apertures will each see a slightly different segment of the return signal. Or one receiver can be translated past an object, taking multiple images along the way [7-16]. The object can either be illuminated by scanning a coherent beam across the target, or by steering the beam to keep the target illuminated. Another approach is to use an array of receivers with multiple transmitter locations [1]. Each transmitter location will increase the angular spectrum content seen by the receivers by looking at the target from different angles.

For each of these systems the sub-apertures need to be aligned relative to each other to create a larger effective aperture. For translated receiver arrays and multiple transmitter location systems, redundant information is captured by overlapping the receiver positions. This redundant information can then be matched up to align the segments of the signal return. One way to determine the relative location of each aperture is to maximize the speckle correlation peaks.

In order to synthesize the apertures together using the speckle it is necessary to measure the reflected signal field. A common way to accomplish this is through coherent spatial heterodyne detection. Mixing the signal with a local oscillator (LO) produces interference fringes in the pupil plane. From the intensity fringes recorded by the digital camera the signal field can be isolated in post processing [1-3, 8-10]. The signal field segments from multiple apertures can then be stitched together to form a synthetic image. The digital holographic process will be described in more detail in chapter 2.

## 1.2 Previous Work

The angular resolution of long range remote sensing systems is proportional to the wavelength used to illuminate the target. It is also inversely proportional to the receiver aperture diameter [17]. Synthetic aperture radar (SAR) systems seek to improve resolution by translating a point detector past a target and capturing multiple shots. In post processing the sub-shots are merged to create a larger synthetic detector. Increasing the size of the effective receiver diameter increases the longitudinal cross-range resolution. However the transverse cross-range resolution remains limited by a single aperture diameter. Increasing the resolution using a larger synthetic aperture is called aperture gain [1].

Synthetic aperture ladar (SAL) uses the same principals as SAR except at smaller optical wavelengths, which also increases the resolution. Both SAR and SAL can use either point detectors or two dimensional detector arrays. Multiple wavelengths and a two dimensional translating detector array can be used to produce three dimensional data (Figure 1) [7-15]. Another option is to translate a single receive aperture using a two dimension translation stage, or translate an array of receive apertures to increase the resolution in both dimensions [16].

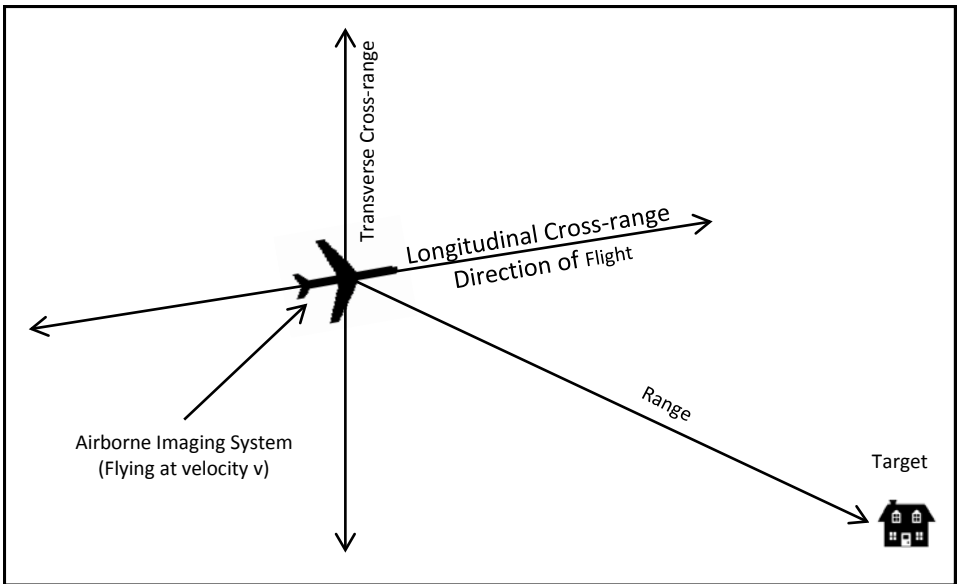


***Figure 1: Basic SAR/SAL Coordinates***

Modern detectors, such as photographic film or charge coupled devices (CCD), can only directly measure the intensity of the returning signal. The signal field is required to align the sub-apertures to create a synthetic aperture. Spatial heterodyne detection uses holographic techniques to measure the signal field. If the signal is mixed with a LO on a CCD then the signal field in the pupil plane can be extracted digitally in post processing [1-3, 8-10]. Mathematical transforms have been developed to estimate the relative locations of each signal field segment using prior knowledge of the physical location of the sub-apertures when the images were recorded [8-10].

Rabb et al. used an array of three receive apertures, and a moving transmitter to capture multiple views of a target [1]. Moving the transmitter relative to the receiver array adds a tilted phase term to the illumination beam at the target. This causes a translation of the reflected signal in the pupil plane. The receivers record the intensity the reflected signal mixed with a LO. This is analogous to moving the receive aperture to view new sections of the speckle field. The transmitter

locations are spaced such that the reflected signal translates less than a full aperture width. The receive apertures will capture duplicate information for each transmitter location. The signal field is determined using digital holography and then the duplicate field segments can be used to align the array to produce a synthetic aperture. The final image will have improved resolution due to aperture gain. [1]

An approach to align the fields in the pupil plane is to use overlapping speckle cross-correlation to find the relative position and phase differences between apertures [1, 7 & 8]. From there the position and phase of each aperture can be adjusted which accounts for any vibration of the transceiver without monitoring the relative location of each sub-aperture during data collection. For the work presented here a bi-static spatial heterodyne ladar system will be utilized where the overlapping regions of the sub apertures are registered using a speckle cross-correlation algorithm. This work applies for any system that captures overlapping sub-apertures, whether using SAL or multiple transmitter locations.

## 1.3 Problem Statement

All of the previous work has been done using high transmitter power. This was primarily done to overcome the noise floor associated with CCD cameras and to ensure that the reflected signal was not completely absorbed by the atmosphere. The objective of this work was to examine the influence of low signal to noise ratios (SNR) on the aperture synthesis process. In this case the system was shot noise limited and atmospheric effects were ignored.

The system will be more convenient for real world applications if the transmitter power necessary to synthesize high quality images is low. Investigating the errors from registering the sub-apertures at low SNR will also demonstrate how accurately the speckle cross-correlation algorithm aligns the synthetic aperture. Tippie and Fienup determined that for a shot noise limited single shot digital holography system a recognizable image could be recovered in very weak signal situations [17]. It is conceivable that with a synthetic aperture the signal could be even weaker and still reconstruct the image. However that is only possible if the registration program used to piece together the synthetic aperture does not add too much extra noise. This work seeks to demonstrate that there are limitations in the accuracy of the registration program, but that the errors are small enough to allow the synthetic aperture system to produce high resolution images in photon starved situations.

# 2 THEORY

## 2.1 Digital Coherent Ladar

A typical long range heterodyne bi-static laser radar (ladar) system splits the output power from a single coherent laser to create a transmitter (TX) and a LO with the same wavelength, phase, polarization and coherence length. The TX flood illuminates a target in the far field at a range z. The reflected signal propagates from the target and into a beam splitter that mixes the signal with the LO. The LO and Signal are coherently mixed to produce an interference fringe pattern on the CCD camera receiver (RX). Figure 2 shows two implementations of the LO. Typically the LO is mixed with the signal using a beam splitter, which produces a complete ladar system on a single platform (Figure 2a).

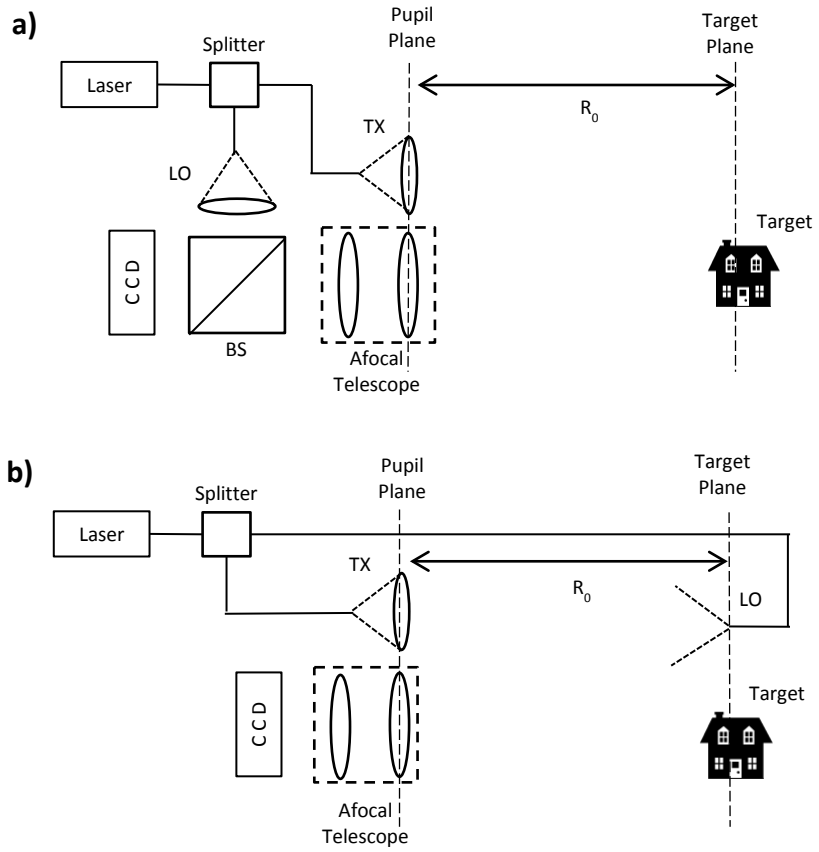


***Figure 2: Ladar System with a) LO Coupled Using a Beam Splitter and b) LO as a Point Source in the Target Plane***

An alternate system is shown in Figure 2b. Here the LO is a point source in the target plane which guarantees that the LO and signal are mode matched at the pupil plane. The LO and the reflected signal propagate the same distance and have the same radius of curvature, and are mode matched in the pupil plane. If the two beams are mode matched, the mixing efficiency will be higher. Once recorded, the fringes are inverse Fourier Transformed to propagate them to the image plane. If the LO is a tilted plane wave, or a point source off axis in the far field target plane, then the terms in the image plane will be spatially separated. Therefore the signal field can be extracted from the fringes, as can be seen below.

The intensity recorded by the RX, signified below as I, is the modulus squared of the LO and object fields added together (Equation (1)). The target field is denoted by f and the LO point source field is g, in the target plane. The Fourier Transform of f and g are denoted by F and G, respectively, and represent the fields in the far field at the pupil plane. The intensity of the interference fringes, I, is recorded digitally by the CCD. The inverse Fourier Transform of the intensity propagates the data to the image plane (Equation (2)). This is the same as applying a digital lens to the system. In Equation (2), $\mathcal{FT}^{-1}\{\}$ is the inverse Fourier Transform operator, $\circledast$ represents convolution, and $^*$ represents the complex conjugate of the field.

$$I = |F + G|^2 = |F|^2 + |G|^2 + F^*G + FG^* \tag{1}$$

$$\mathcal{FT}^{-1}\{I\} = f \circledast f^* + g \circledast g^* + f^* \circledast g + f \circledast g^* \tag{2}$$

If the LO is implemented as a point source or a delta function in the target plane located at ($x_{LO}$, $y_{LO}$), with an amplitude equal to the square root of the intensity $I_{LO}$, then Equation (2) becomes Equation (3). Notice in Equation (3), the first term is the autocorrelation of the signal field centered at the origin. The second term is the autocorrelation of the LO, which is just a delta function at the origin. Typically the LO intensity is much stronger than the signal intensity. Therefore the second term will dominate the first at the origin. The last two terms are image terms that are spatially separated, one located at ($x_{LO}$, $y_{LO}$) and the other at (-$x_{LO}$, -$y_{LO}$). The image terms are complex conjugates of each other and can be isolated. [19]

$$\mathcal{FT}^{-1}\{I\} = f \circledast f^* + I_{LO}\delta(x,y) + \sqrt{I_{LO}}\, f(x - x_{LO}, y - y_{LO}) + \sqrt{I_{LO}}\, f^*(x + x_{LO}, y + y_{LO}) \tag{3}$$

To demonstrate how the signal field can be digitally extracted, consider a one dimensional system with a point object in the target plane located at x = a, and another point source located at x = b acting as the LO. Let the amplitude of each of these fields to be equal to the square root of their intensities ($I_o$ and $I_{LO}$). Then the object and LO fields can be written using Equations (4) & (5). A relative phase, $\phi$ has been included on the object to represent any phase variations.

$$f(x) = \sqrt{I_o}\, \delta(x - a)\, e^{j\phi} \tag{4}$$

$$g(x) = \sqrt{I_{LO}}\, \delta(x - b) \tag{5}$$

Assuming the target is in the far field, the Fourier Transform is applies to propagate these fields to the pupil plane (Equations (6) & (7)) [20]. Here the coordinate used in the pupil plane is $\xi$, to avoid confusing it with the coordinate, x, in the target plane. Figure 3 demonstrates the coordinate systems used in this work for each conjugate plane: target plane, pupil plane and image plane. Information can be propagated between conjugate planes using Fourier Transforms assuming there are far enough away to approximate the far field. For a physical system with a lens in the pupil plane, an image is produced in the focal plane. For digital holography, a digital lens is applied by Fourier Transforming the intensity recorded in the pupil plane to the focal or image plane. Therefore in this work both the image and target planes are located at the same place, and will use the same coordinate system of (x, y).

$$F(\xi) = \sqrt{I_o}\, e^{\left(j\phi - j\frac{k}{z}\xi a\right)} \tag{6}$$

$$G(\xi) = \sqrt{I_{LO}}\, e^{-j\frac{k}{z}\xi b} \tag{7}$$

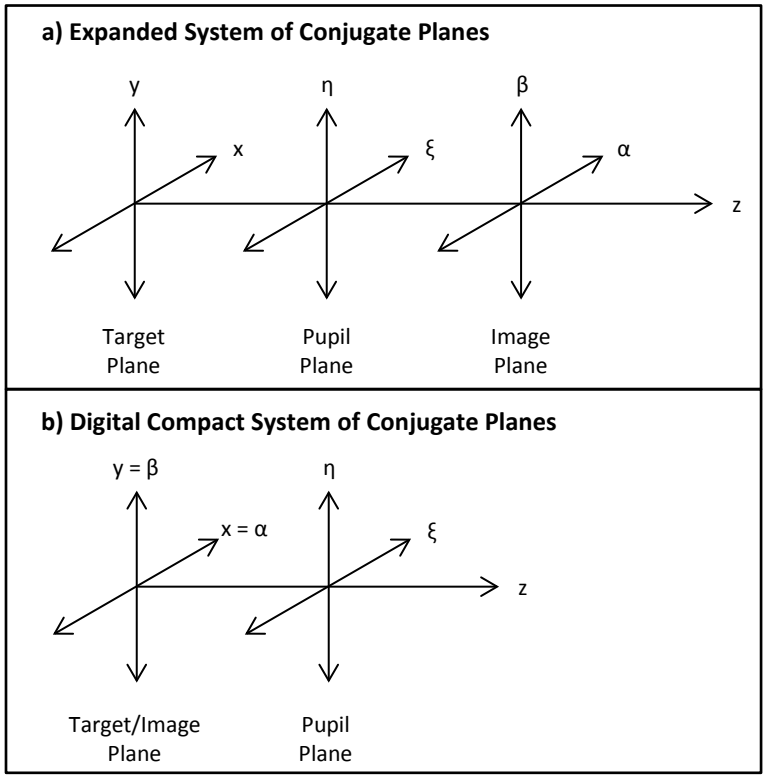


***Figure 3: Coordinate Systems for an a) Expanded and b) Compact System***

Using Equation (1), the interference fringe intensity at the detector from mixing the point target and LO can be written as Equation (8). The relative phase difference between the signal and LO fields is $\Phi(\xi)$ (Equation (9)) [19].

$$I(\xi) = |F(\xi) + G(\xi)|^2 = I_o + I_{LO} + \sqrt{I_o I_{LO}}\left(e^{j\Phi(\xi)} + e^{-j\Phi(\xi)}\right) \tag{8}$$

$$\Phi(\xi) = \phi - \frac{k}{z}\xi(a - b) \tag{9}$$

The incident power can be converted to detector output signal in photoelectrons by multiplying by the quantum efficiency of the detector, QE, and the integration time, $\tau$, and dividing by the energy per photon, $h\nu$. Where h is Plank's constant and $\nu$ is the frequency of the light. The detector output is shown in Equation (10). An additional noise bias term, $P_B$, has been added to account for background noise. The background noise could be due to camera noise or any other sources of light besides the signal that fall on the CCD.

$$d(\xi) = \frac{(QE)\tau}{h\nu}(P_S + P_{LO} + P_B) + \frac{(QE)\tau}{h\nu}\sqrt{P_S P_{LO}}\left(e^{j\left(\phi - \frac{k}{z}\xi(a-b)\right)} + e^{-j\left(\phi - \frac{k}{z}\xi(a-b)\right)}\right) \tag{10}$$

$$\begin{aligned} D(x) &= \mathcal{F}\{d(\xi)\} \\ &= \frac{(QE)\tau}{h\nu}(P_S + P_{LO} + P_B)\delta(x) + \frac{(QE)\tau}{h\nu}\sqrt{P_S P_{LO}}\left(e^{j\phi}\delta\left(x - \frac{k}{z}(a-b)\right)\right) \\ &+ \frac{(QE)\tau}{h\nu}\sqrt{P_S P_{LO}}\left(e^{-j\phi}\delta\left(x + \frac{k}{z}(a-b)\right)\right) \end{aligned} \tag{11}$$

Taking the Fourier Transform of the output from the CCD propagates the information to the image plane (Equation (11)). Notice that Equation (11) has the same form as Equation (3). The last two terms are spatially separated. Therefore in order to extract the signal field, simply crop out one of the last two terms. This can be done by evaluating Equation (11) at Equation (12), to find Equation (13). [19]

$$x_{crop} = \frac{k}{z}(a-b) \tag{12}$$

$$D(x_{crop}) = \frac{(QE)\,\tau}{h\nu}\sqrt{P_S P_{LO}}\, e^{j\phi} \tag{13}$$

## 2.2 Noise Sources and Signal to Noise Ratio

There are a variety of possible noise sources in synthetic aperture ladar imaging systems. Noise is any random fluctuations in the number of photons or photoelectrons that are measured on or from the detector. Noise can come from the detector in the form of shot noise, dark noise and thermal noise. There is background noise from light scattering off other surfaces besides the target and any other sources of light incident on the detector. There can also be fluctuations in the phase of the signal due to relative motion of the target, TX or RX. Any longitudinal motion between the target and the RX will cause the speckle pattern on the camera to move, this will be discussed further in Chapter 4. Noise can come from optical components before the detector and the electrical components after the detector. Another large noise source is the atmosphere that the laser light travels through. In this work, atmospheric effects will be neglected.

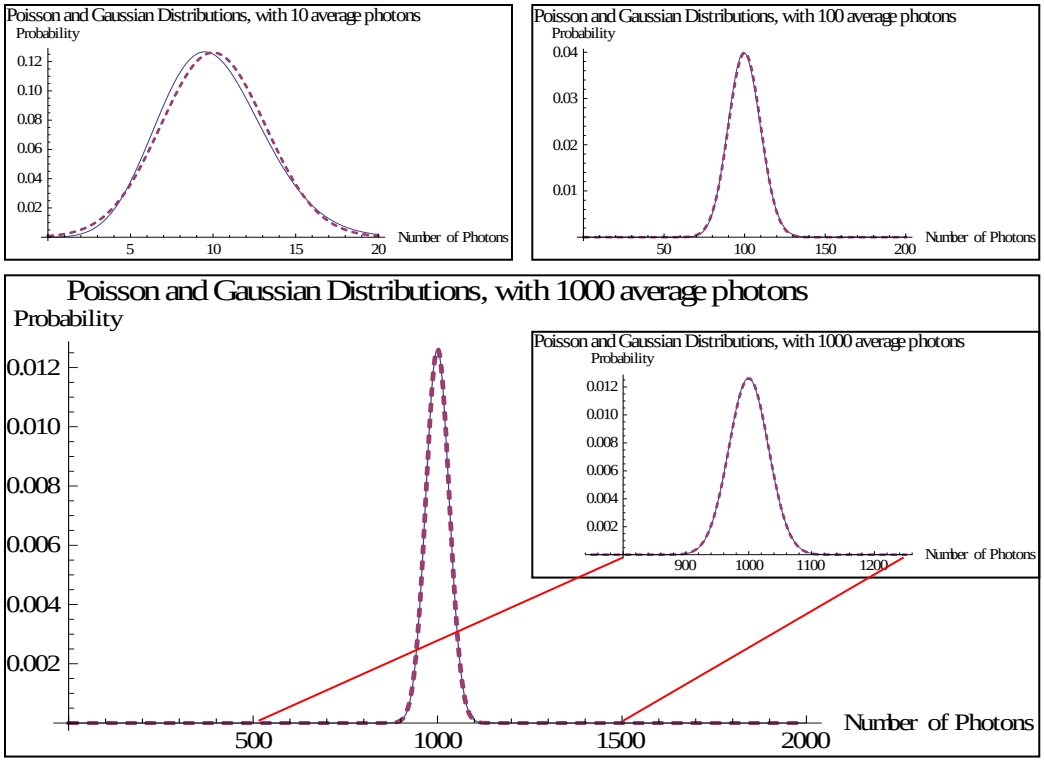


***Figure 4: Plots of Poisson vs. Gaussian Probability Distributions***

Each noise source has its own statistical average and probability distribution. Shot noise describes the fluctuations due to the random nature of detecting optical signals. Sometimes it is attributed to the discrete photon energies and the uncertainty in the time each of these photons is detected. Shot noise has a Poisson probability distribution, which approaches a Gaussian distribution for a large number of photons. Figure 4 demonstrates how a discrete (dashed line) Poisson distribution, as a function of the number of samples n, with an average value μ (Equation (14)) can be approximated by a continuous (solid line) Gaussian distribution, with an average μ equal to the variance $\sigma^2$ (Equation (15)) for a large number of samples, or in this case photons [31]. For this work, the LO at half well capacity illuminates the CCD with over 100,000 photons per pixel, thus the shot noise is Gaussian distributed.

$$P_{\mu}(n) = \frac{\mu^n}{n!} e^{-\mu} \tag{14}$$

$$G_{\mu,\sigma}(n) = \frac{1}{\sqrt{2\pi\sigma^2}} e^{-(n-\mu)^2/2\sigma^2} \tag{15}$$

The shot noise can be written in terms of the variance in the photo-current from the detector, i. The photo-current can be calculated from the received optical power, $P_R$, using Equation (16). The average photo-current from the signal is $i_s$, and the variance of the photo-current due to the signal shot noise is $\langle i_{shot,S}^2 \rangle$ (Equation (17)). The charge of an electron is e, and B is the bandwidth of the circuit, or the inverse of the integration time. Similarly, shot noise due to the background, $\langle i_{shot,B}^2 \rangle$, and the dark current, $\langle i_{shot,D}^2 \rangle$, can be written as Equations (18) & (19). [19]

$$i_S = \frac{QE\ e}{h\nu} P_R \tag{16}$$

$$< i_{shot,S}{}^2 >= 2eB < i_s > \tag{17}$$

$$< i_{shot,B}{}^2 >= 2eB < i_B > \tag{18}$$

$$< i_{shot,D}{}^2 >= 2eB < i_D > \tag{19}$$

Thermal noise is caused by fluctuations due to the temperature of the detector. It depends on the temperature, T, Boltzmann's constant, k, and the resistance of the circuit, R. Thermal noise is Gaussian distributed. The variance of the photo-current due to thermal noise is described by Equation (20) [19].

$$< i_T{}^2 >= \frac{4kTB}{R} \tag{20}$$

The SNR can be calculated by dividing the variance in the signal photo-current by the variances due to the noise sources (Equation (21)) [19]. This assumes that the noise sources are statistically independent such that the variances can simply be added to find the total noise.

$$SNR = \frac{< i_S >^2}{< i_{shot,S}{}^2 > + < i_{shot,B}{}^2 > + < i_{shot,D}{}^2 > + < i_T{}^2 >} \tag{21}$$

If the system is signal shot noise limited, the shot noise due to the signal will dominate and the SNR simplifies to Equation (22), using Equations (16) & (17). [19]

$$SNR = \frac{< i_S >^2}{< i_{shot,S}{}^2 >} = \frac{\left(\frac{QE\ e < P_R >}{h\nu}\right)^2}{2eB\frac{QE\ e < P_R >}{h\nu}} = \frac{QE}{2Bh\nu} < P_R > \tag{22}$$

## 2.3 Speckle Cross-Correlation Registration

There are various applications where two images, from a translated object, captured using coherent detection methods need to be aligned to increase resolution by creating a synthetic aperture. A method well cited in the literature, is to cross-correlate the speckle fields from two pupils and use the peak location and phase to determine the relative translation and piston phase differences between the two images [7]. This is a difficult computational problem due to the large arrays needed to accurately find the correlation peak. Guizar-Sicairos et. al. describe ways to make the computation more efficient [21]. The algorithm used was developed using the principles below.

Two overlapping portions of the interference fringes are captured in the pupil plane. These two portions could be captured by translating the receiver, or by rotating the object, or by changing the location of the transmitter relative to the receiver. Whichever method is used to collect the

data, there will be a relative phase and translation difference between the two apertures. The two portions are digitally processed to isolate two overlapping sections of the object field in the pupil plane. The overlapping region is cropped from each section and will be represented by $F_1$ & $F_2$. Equation (23) shows the second overlapping field region in terms of the shifted first region. Only the duplicated regions are represented. The coordinate vector for the pupil plane is $\vec{R} = \vec{\xi} + \vec{\eta}$.

$$F_2(\vec{R}) = F_1(\vec{R} - \vec{S})\, e^{\frac{jk}{z}(\vec{T}\cdot\vec{R})+j\phi} \tag{23}$$

The vector $\vec{S}$ describes the translation between $F_1$ & $F_2$ in the pupil plane. The translation vector,$\vec{T} = (T_\xi, T_\eta)$, in the image plane and the phase difference, $\phi$, describe the adjustments necessary to align the segments into a synthetic aperture.

$$\begin{aligned}(f_1 g^* \circledast f_2 g^*)(\vec{u}) &= \mathcal{FT}^{-1}\{(F_1 G^*)(F_2 G^*)\} \\ &= \mathcal{FT}^{-1}\left\{F_1(\vec{R})G^*(\vec{R})F_1(\vec{R} - \vec{S})\, e^{\frac{jk}{z}(\vec{T}\cdot\vec{R})+j\phi}G^*(\vec{R})\right\}\end{aligned} \tag{24}$$

Equation (24) shows the cross-correlation of the image components of the data captured by the receiver using coherent detection. The vector $\vec{u}$ describes the shift between $f_1 g^*$ and $f_2 g^*$. Here the cross-correlation has been written in terms of the pupil plane fields, $F_1$ & $F_2$, according to the convolution theorem [20]. In the second line of Equation (24), Equation (23) has been substituted for $F_2$. Note that the reference beam, G, is equal for both apertures because a point source for the LO is uniform across the pupil plane in the far field.

If the translation between the apertures, $\vec{S}$, is much smaller than the size of a speckle in the pupil plane then $F_1(\vec{R} - \vec{S}) \approx F_1(\vec{R})$, and Equation (24), reduces to Equation (25). Using the convolution theorem, the multiplication of the pupil plane pieces can be written as the convolution of the image plane pieces (Equation (26)). A phase tilt in the pupil plane is the same as a translation in the image plane. Therefore the cross-correlation of the two overlapping image segments is the same as the autocorrelation of the reference segment with piston phase and translation adjustments. [7]

$$\begin{aligned}(f_1 g^* \circledast f_2 g^*)(\vec{u}) &= \mathcal{FT}^{-1}\left\{\left(F_1(\vec{R})\right)^2\left(G^*(\vec{R})\right)^2 e^{\frac{jk}{z}(\vec{T}\cdot\vec{R})+j\phi}\right\} \\ &= e^{j\phi}\left[\mathcal{FT}^{-1}\left\{\left(F_1(\vec{R})\right)^2\left(G^*(\vec{R})\right)^2\right\} \times \mathcal{FT}^{-1}\left\{e^{\frac{jk}{z}(\vec{T}\cdot\vec{R})}\right\}\right]\end{aligned} \tag{25}$$

$$(f_1 g^* \circledast f_2 g^*)(\vec{u}) = e^{j\phi}\left[(f_1 g^* \circledast f_1 g^*)(\vec{u}) \circledast \delta(\vec{u} - \vec{T})\right] = e^{j\phi}\left[(f_1 g^* \circledast f_1 g^*)(\vec{u} - \vec{T})\right] \tag{26}$$

As long as the correlation peak can be accurately located, the relative piston and tilt adjustments needed to align the segments can be determined. The basic process involved to estimate the peak location is to embed the cross-correlation array in a larger array of zeros, this will up-sample the cross-correlation array when an inverse discrete Fourier Transform (DFT) is applied. By up-sampling the cross-correlation peak, it can be more accurately located.

The algorithm used in this work was developed by Dr. David Rabb and Jason Stafford by modifying the *efficient subpixel image registration by cross-correlation* m-file available for download from MathWorks, Inc. [21 & 22]. Once the correlation peak location has been estimated using the DFT process, a small region around the peak is cropped out and up-sampled to more accurately locate the peak in the original array. This process is repeated for smaller and smaller regions around the peak until the location is known with a specified fraction of a pixel. For this project the peak was up-sampled by a factor of 8, 5 times. The program was set to shift the second array ±4 pixels in both dimensions in search of the maximum correlation peak. For these settings, the program finds the maximum correlation peak with a resolution of 1/8192 of a pixel. By limiting the program to only look for the peak within ±4 pixels in both dimensions, an initial estimation of the peak location has been made. It has been assumed that the two apertures are within ±4 pixels of being aligned. The registration process is used to more accurately synthesize the sub-apertures.

Once the cross-correlation peak has been pinpointed, the relative piston phase and tilt errors between the sub-apertures can be calculated. The program that was used reports the piston phase errors in radians, and the tilt errors in terms of translation in the image plane. If the pupil and image planes are conjugate planes, then a translation in one plane appears as a phase tilt in the opposite plane. Therefore any row and column translations in units of pixels, in the image plane, correspond to phase tilts in the pupil plane in units of waves of tilt across the aperture.

## 2.4 Modulation Transfer Function

The modulation transfer function (MTF) is a quantitative measurement of the image contrast transfer function of an imaging system. It is a function of the spatial frequency of the object. The MTF can be used to define how well an imaging system transfers the contrast of the object to the image. For this work, the MTF will be used as a metric for image quality.

To calculate the MTF for this system, a point target will be simulated in Chapter 5. This will allow the MTF to be determined for every spatial frequency in one step. For a single frame captured by an aperture with a diameter D, the diffraction limited spatial frequency bandwidth is $f_0$ (Equation (27)) [20]. Where the wavelength of the TX laser is $\lambda$, and the range to the target is z.

$$f_0 = \frac{D}{\lambda z} \tag{27}$$

For a single aperture, where the CCD RX diameter is 7.7 mm the wavelength is 1545 nm and the range is 2 m, the bandwidth is 2.5 cycles per millimeter (cyc/mm). If two sub-apertures are overlapped by half a diameter and combined into a synthetic aperture then the synthetic aperture diameter would be 1.5 * 7.7 mm = 11.55 mm. This synthetic aperture increases the spatial frequency bandwidth to 3.74 cyc/mm.

The MTF for an incoherent system with a square aperture is a triangle function that extends linearly between an MTF of 1 at zero cyc/mm and the spatial frequency bandwidth limit at an MTF of zero. For a coherent system the MTF for a square aperture is a rectangle function [20]. Although the system used for this work uses coherent illumination to image the target, the intensity data is filtered by the incoherent transfer function. This transforms the MTF from a

rectangle function for a single image, into a triangle function for the incoherent intensity image. The MTF of the simulated or experimental data can be found using the single or synthetic aperture image. The first step is to take the Fourier Transform of the image. The intensity point spread function (PSF) is the modulus squared of this Fourier Transform. Next Fourier Transform the PSF to calculate the spatial frequency content. The MTF is the normalized central slice of the spatial frequency content.

# 3 SIMULATION

The goal of the simulation is to estimate the effects of low SNR on the registration process and the MTF. To be effective requires that the simulation mimic as many of the physical aspects of the ladar system as possible. The ladar system that was investigated is described in the first section of this chapter to explain the characteristics of the simulation. The dominant noise sources can be modeled to explain the registration errors found in the laboratory at low SNR. The simulation was divided into two sections to simplify the programming. The first section, described in this chapter, models the laboratory experiment to determine what results are expected. Both the processed data and the simulation output the root-mean-square (RMS) registration errors as a function of signal levels. The second section, described in Chapter 5, examines the effect of the registration errors on the MTF of the system.

## 3.1 Experimental Design

A schematic of the experiment can be seen in Figure 5. This set up was a bi-static homodyne coherent laser imaging system. The basic operation of the set up involves a transmitter (TX) aimed at a reflective target. The reflected signal mixes with the local oscillator (LO) on the receiver (RX). The interference fringes on the receiver were digitally recorded and the signal field was extracted in post processing. The plane of the target and LO is called the Target Plane and is the same as the Image Plane (Figure 6a). The plane of the TX and the RX is the Pupil Plane (Figure 6b). The Target/Image Plane is positioned 2 m away from the Pupil Plane. This range violates the far field assumption used in Chapter 2. However the LO and reflected signal were flat in the pupil plane over the RX, so the far field equations still apply. Any specular reflections from the target were directed away from the receiver.

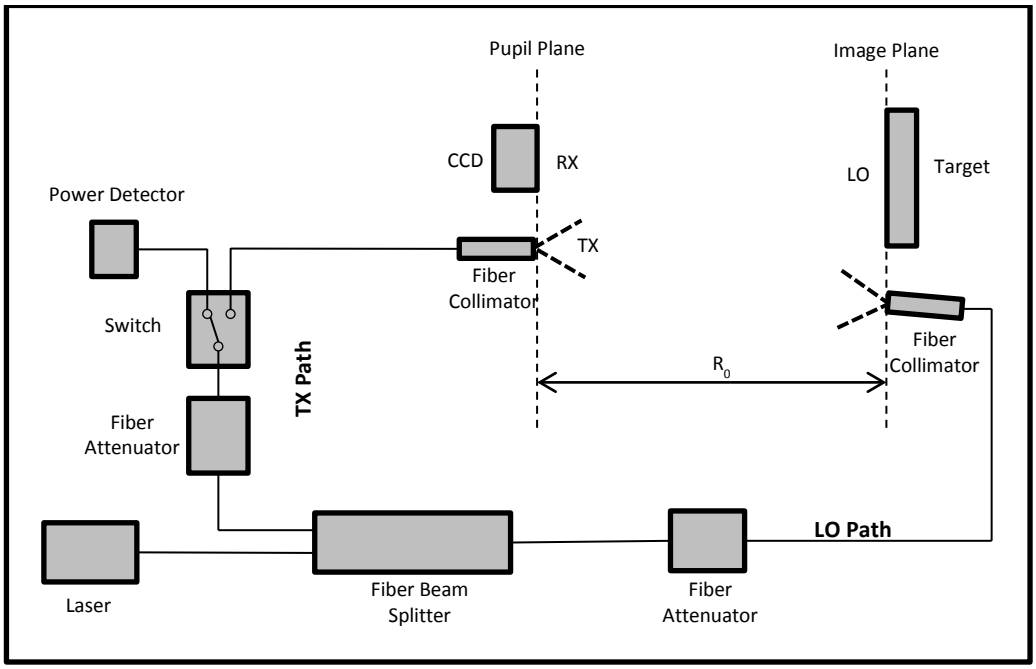


***Figure 5: Schematic of the Experimental Set-up***

*a)* 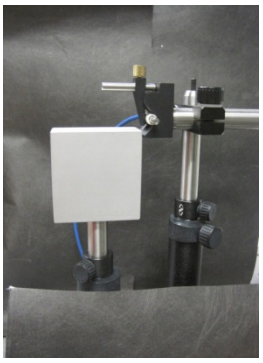 *b)* 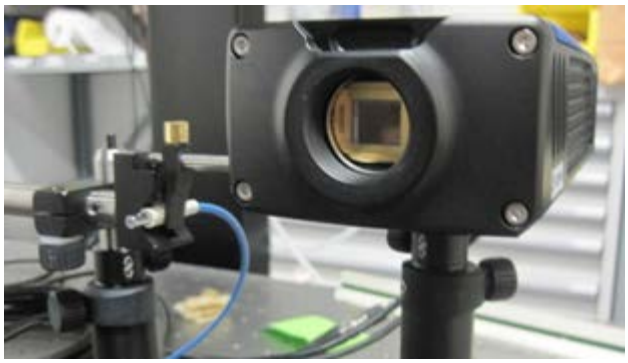

***Figure 6: Images of the a) Target Plane and b) Pupil Plane from the Actual Experiment***

The LO and TX in this system use the same laser so that they have the same wavelength, phase, and polarization which increases the mixing efficiency when they interfere. Also the LO was transmitted from the Image Plane so that it has the same radius of curvature as the reflect signal in the Pupil Plane. Mode matching the interfering waves increases the mixing efficiency for coherent interference.

The laser used was a Redfern Integrated Optics (RIO) Orion laser module which housed an external cavity laser diode. The laser has a continuous wave output power up to 20 mW, a wavelength of 1545 nm and a spectral linewidth less than 3 kHz [23]. The laser was connected by polarization maintaining optical fibers to an Oz Optics miniature inline splitter. All of the fibers used in this experiment were single mode polarization maintaining (PM) with a Panda configuration [24]. The miniature inline fiber splitter has one input port and two output ports (Figure 7). The splitter passes 96% of the laser power to output fiber 1, while the other 4% of the power is reflected to output fiber 2 [25].

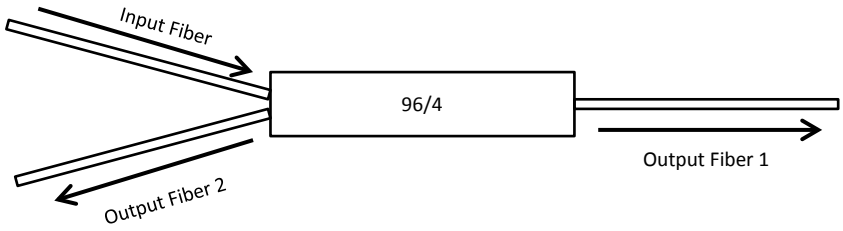


***Figure 7: A Schematic and Picture of the Inline Fiber Splitter***

Most of the laser power was used for the LO to guarantee that the set up was shot noise limited. Therefore output fiber 1 was connected to an inline variable attenuator and then a pigtail style collimator. The fiber collimator had an output beam diameter of 0.2 mm and was mounted off axis in the image plane and directed toward the receiver to act as the LO [26]. The LO was

placed next to the corner of the target and as close to the same plane as possible to ensure mode matching. Output fiber 2 was connected to an inline variable attenuator as well in order to set the TX to low power levels.

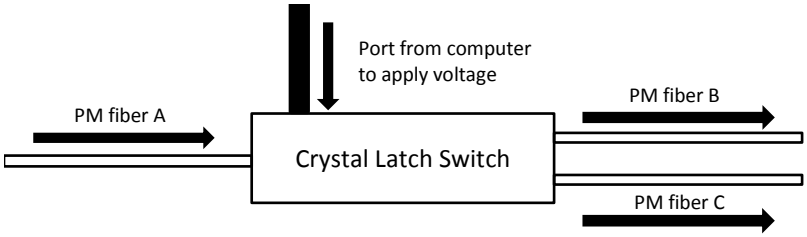


***Figure 8: Schematic of the Switch Used to Turn the TX On and Off***

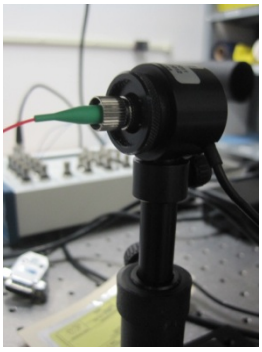

***Figure 9: Nova II Power Detector with Fiber Connector***

The TX path was then connected to an Agiltron crystal latch switch with one input (fiber A) and two output fibers (B and C) (Figure 8). The switch was non-mechanical and activated using a low voltage signal. Even after the voltage had been removed the switch maintained its configuration [27]. The first output (fiber B) from the switch was connected to a pigtail style collimator with an output beam diameter of 0.2 mm [26]. The collimator was then mounted in the Pupil Plane to act as the TX.

The second switch output (fiber C) was connected through a fiber connector to an InGaAs Ophir Nova II power detector (Figure 9) [28]. The switch was manually flipped using Agiltron software. When the power was set to pass from fibers A to B then the TX was turned on and interference fringes can be recorded. Whereas if the power was set to pass from fibers A to C then the power could be measured by the Nova II but only the LO power was received by the RX. This allowed for repeated measurements of the transmit power without having to place a detector in the middle of the system.

The target used was an anodized aluminum block that was found to be highly reflective at 1545 nm (Figure 10). The 2 inch square face of the block was subjected to an abrasive blasting of glass beads to produce a rough surface. The TX was aligned with the center of the block. The receiver was aligned on the same optical axis as the target and at the same height 2 m away. The receiver used was a FLIR SC2500 thermal camera. The camera was operated without a filter or a lens. Therefore the only thing between the bare CCD detector and the target was a cover glass. The FLIR SC2500 has an InGaAs detector with a spectral range of 0.9-1.7 μm [29]. The camera was windowed down from 320 x 256 pixels to 256 x 256 pixels using a built in digital control.

With a pixel pitch of 30 μm, the receive aperture diameter was 7.7 mm. The frame rate of the camera was set to 120 Hz with an exposure time of 100 μs. The signal from the CCD was read via snapshot mode into a computer using LabVIEW. The raw data was saved and processed in Matlab. The process for setting the signal level and processing the experimental data will be explained in the next chapter.

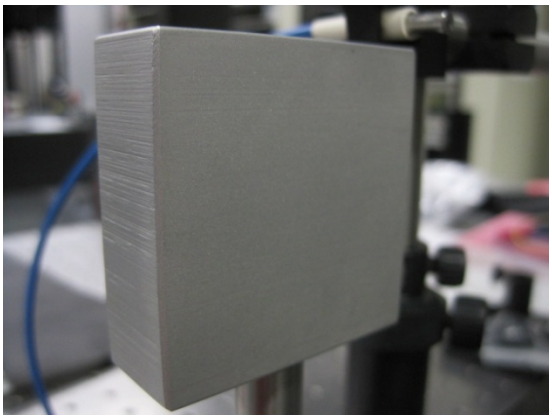

***Figure 10: Rough Surface Target***

For each signal level multiple images of the interference fringe patterns were captured. The adjacent frames were plugged into a speckle cross-correlation registration algorithm. Typically this algorithm would be used to align frames that had been captured from multiple angles or positions. In that case the output from the algorithm would be the piston phase, tip and tilt adjustments that if applied to one of the apertures, would align it with another. For the set-up used here, the apertures are not moved between frames. Therefore the piston phase, tip, and tilt adjustments should be zero. Any adjustments that are not exactly zero are therefore errors in the registration caused by the varying shot noise between frames.

## 3.2 Programming Steps

The simulation begins by modeling a rough target with the same dimensions as in the laboratory experiment. The speckle produced by illuminating a rough surface with a coherent beam can be simulated by creating a circularly complex Gaussian random distribution over the target area (Figure 11). In this case a random number between zero and one was chosen using a circularly complex Gaussian probability distribution. A circularly complex Gaussian distribution has statistically independent Gaussian random variable distributions for both the real and imaginary parts of the target [30]. This probability distribution accurately models a large sum of random phasors where each point on the rough surface contributes to the phasor sum.

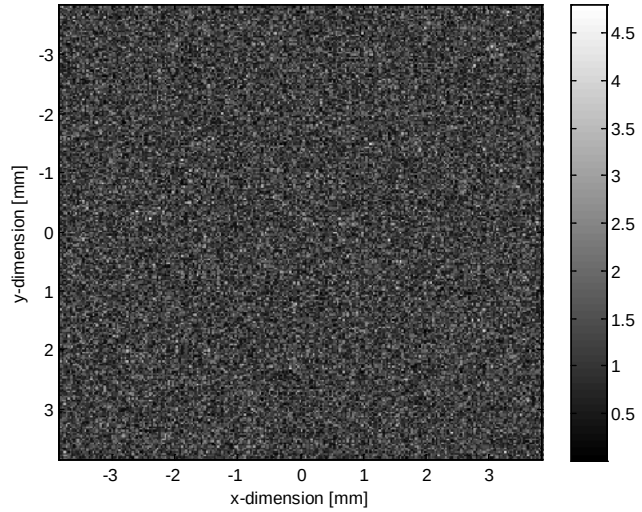


***Figure 11: Circularly Complex Gaussian Speckles in the Target Plane***

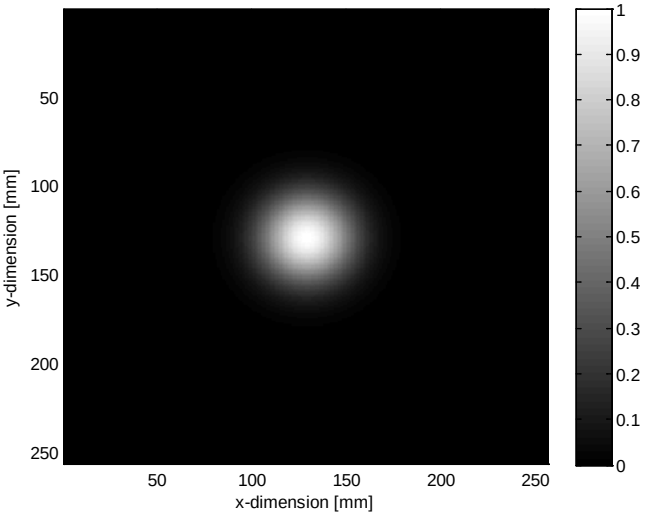


***Figure 12: Gaussian Mask Applied to the Target***

Before propagating this target to the pupil plane, a Gaussian mask was applied to simulate the Gaussian beam shape of the transmit beam on the reflective target (Figure 12). The beam waist of the Gaussian intensity mask was set 9.8 mm at the target. This value was found using the standard Gaussian beam radius equation as a function of range, with $w_0$ equal to 0.1 mm (Equation (28)). The rough target field was multiplied by the square root of the mask and propagated to the pupil plane by applying a Fourier Transform (Figures 13 & 14).

$$w(z) = w_0 \sqrt{1 + \left(\frac{z\lambda}{\pi {w_0}^2}\right)^2} \tag{28}$$

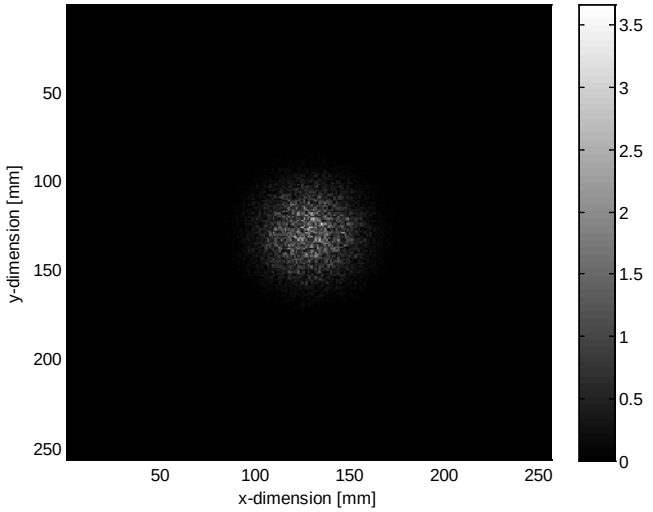


***Figure 13: Reflected Signal in the Target Plane***

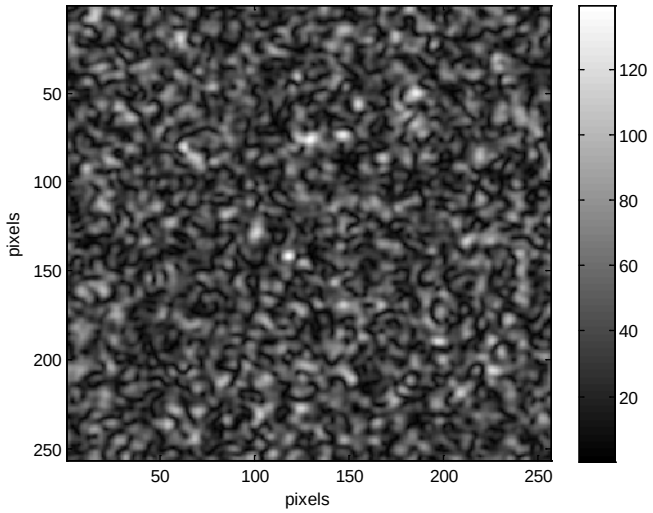


***Figure 14: Reflected Signal in the Pupil Plane***

Once in the pupil plane the average signal value was adjusted to match the desired number of signal photons hitting the RX (Figure 15). Using Equation (29)) the adjusted Signal can be calculated by multiplying the signal field, $A_o e^{j\phi_o}$, by the ratio of the desired average by the original average. Here M is the desired average number of signal photons on the CCD, N is the number of pixels in one dimension on the CCD, and $A_0$ and $\phi_0$ are the original amplitude and phase of the signal field. Therefore M/ ($N^2$) gives the average number of desired signal photons per pixel.

$$\text{Signal} = A_o e^{j\phi_o} \sqrt{\frac{\frac{M}{N^2}}{< |A_o|^2 >}} \tag{29}$$

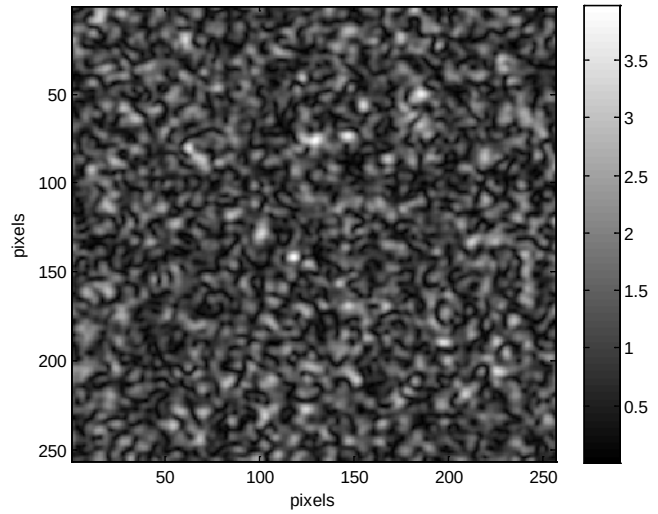


***Figure 15: Signal in the Pupil Plane with 98,750 Photons***

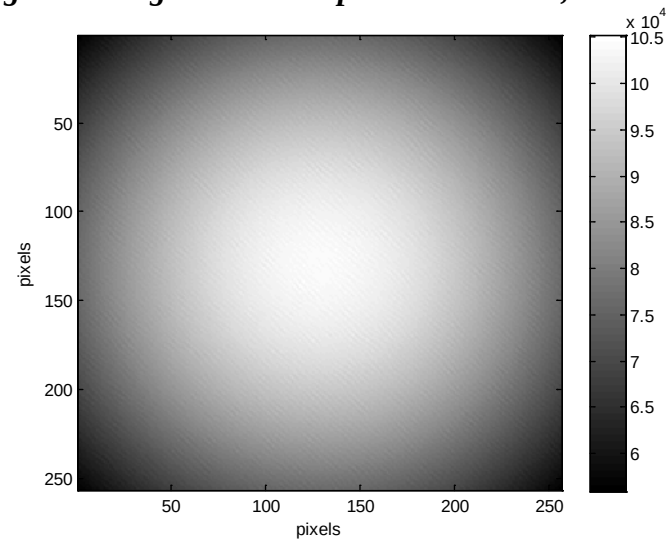


***Figure 16: Half Well Capacity LO in the Pupil Plane***

The LO was created directly in the pupil plane (Figure 16). The LO was created as a tilted plane wave with a Gaussian beam intensity mask to model the Gaussian beam in the experiment (Equation (30)). $A_{LO}$ represents the amplitude of the LO which was set to the half well capacity of the CCD. Half well capacity was chosen to ensure the experimental system was shot noise limited, the same amplitude was used in the simulation for accuracy. The spatial coordinates in the pupil plane are described by $(\xi, \eta)$. The beam waist of the LO Gaussian intensity mask is $w_{LO}$ and was determined to be 9.8 mm using Equation (28).

$$LO = A_{LO} e^{-\left(\frac{\xi^2+\eta^2}{w_{LO}{}^2}\right)} e^{j2\pi \frac{N}{D_{ap}}\left(-\frac{\xi}{4}+\frac{\eta}{4}\right)} \tag{30}$$

The interference fringe pattern was created by adding the LO and signal fields and finding the modulus squared, like in Equation (1) (Figure17). The resulting fringe pattern had a period of 4 pixels. In an effort to mimic the response of the camera in the laboratory, it was necessary to

account for the attenuation of the high frequency components due to the finite extent of the detectors and the unity fill factor of the CCD. Equations (29) & (30) give the maximum value of the signal and LO at each point. In the experiment each pixel will record the average intensity over the square pixel area. The modulation transfer function (MTF) of the square camera pixels is a sinc function, where $\mathrm{sinc}(x) = \frac{\sin(\pi x)}{\pi x}$. For our simulation, the MTF becomes sinc(1/4) = 0.9003 in either dimension, because there is a quarter of a cycle per pixel. Therefore the high frequency components of the fringes are attenuated by $(\mathrm{sinc}(1/4))^2$. This attenuation factor is only applied to the high frequency mixed components (Equation (31)). This assumes that all of the frequencies in the image can be attenuated by one number based on the carrier frequency.

$$\mathrm{Fringes} = |\mathrm{Signal}|^2 + |\mathrm{LO}|^2 + \left(\mathrm{sinc}\left(\frac{1}{4}\right)\right)^2 (\mathrm{Signal}^* \times \mathrm{LO} + \mathrm{Signal} \times \mathrm{LO}^*) \tag{31}$$

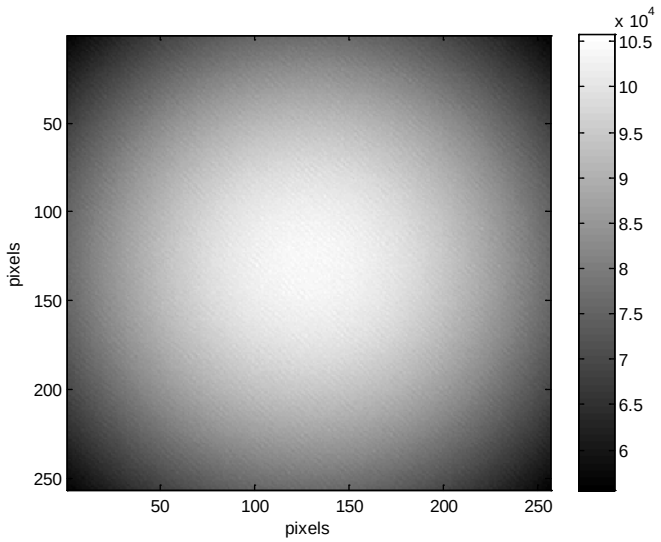


***Figure 17: Intensity of the Signal Mixed with the LO in Units of Photoelectrons***

These fringes were then multiplied by the quantum efficiency, 70%, of the camera to convert to units of photoelectrons. Here it was assumed that the quantum efficiency was constant over the CCD. The fringes were copied to simulate two different frames captured in the same location of a single speckle realization. This imitates two apertures that are overlapped by 100%.

Next, independent shot noise and detector noise was added to each aperture. The noise associated with the detector was added to the simulation to demonstrate that it was always much smaller than the shot noise. Shot noise has a discrete Poisson distributed but approaches a continuous Gaussian distribution for a large number of photons. As discussed in Chapter 2, the LO amplitude was large enough for the shot noise to be estimated by a Gaussian distribution. The shot noise was added as a Gaussian distributed random variable where the average and variance of the distribution were equal to the intensity value at each pixel. The noise for the FLIR SC2500 camera was listed as typically <150 photoelectrons. Therefore the detector noise was modeled as a zero-mean Gaussian distributed random variable with a standard deviation of 150 photoelectrons at each pixel (Figure 18). The detector noise was added even though this system was shot noise limited to demonstrate that it has a negligible effect.

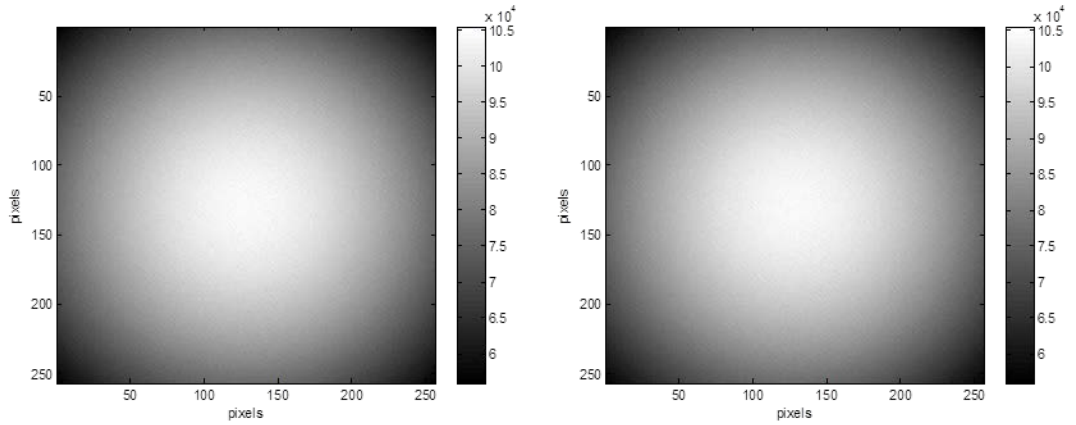


***Figure 18: Two Copies of Intensity Recorded by the RX with Independent Shot Noise***

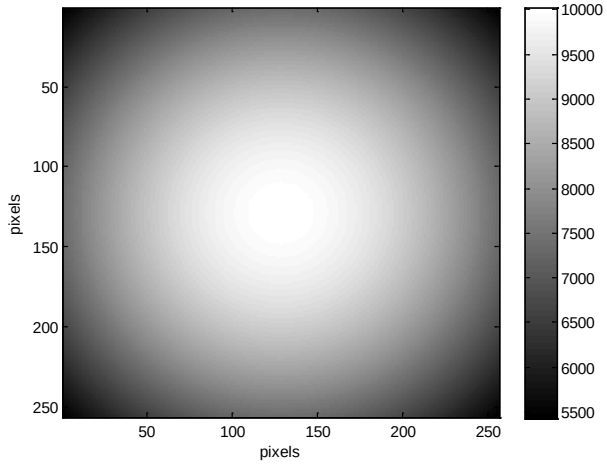


***Figure 19: Simulated LO Recorded by the RX***

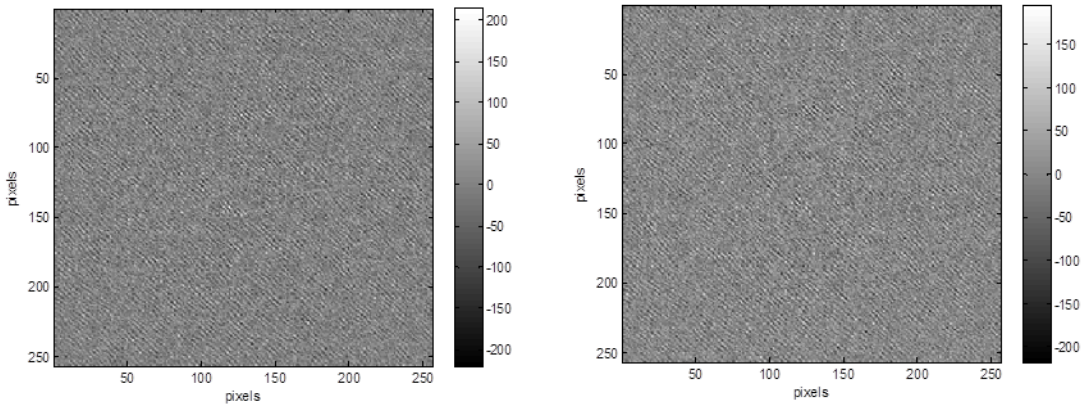


***Figure 20: Two Apertures after Subtracting the Background in Digital Counts***

The two aperture arrays were then converted to units of digital counts to match the experimental data. This was done by multiplying by $2^{14}$ bytes divided by the camera full well capacity in units of photoelectrons, 170,000 e-. The array was then rounded to the next integer value to account

for digitization noise. The last step required to simulate the experimental pupil plane data was to subtract the average LO at each pixel (Figures 19 & 20). In the laboratory experiment the average value over many trials for each pixel was subtracted to factor out static camera and background noise. By doing the same step in the model, the next few steps will be parallel to the steps involved in processing the data.

Once the pupil plane data has been simulated each aperture was inverse Fourier Transformed to the image plane so that the components were spatially separated (Figure 21). The real image component was cropped from the lower left quadrant and Fourier Transformed back to the pupil plane (Figures 22 & 23). The two pupil plane apertures were then plugged into the speckle cross-correlation registration program. The output values are the piston and tilt phase adjustments that need to be applied to the second aperture to line it up with the first aperture. These output values were recorded and the entire process was repeated for 1280 different speckle and noise realizations. The RMS piston and tilt errors were calculated and this entire model was repeated for multiple signal levels.

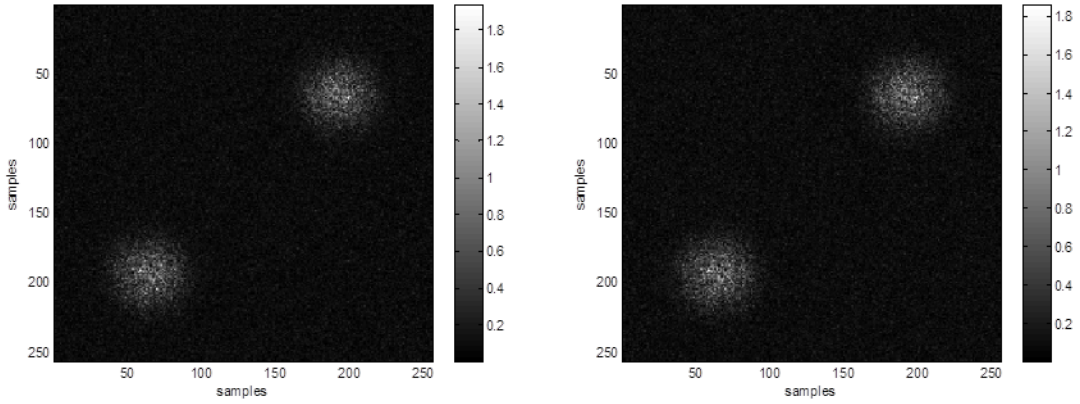


***Figure 21: Images from Each Aperture***

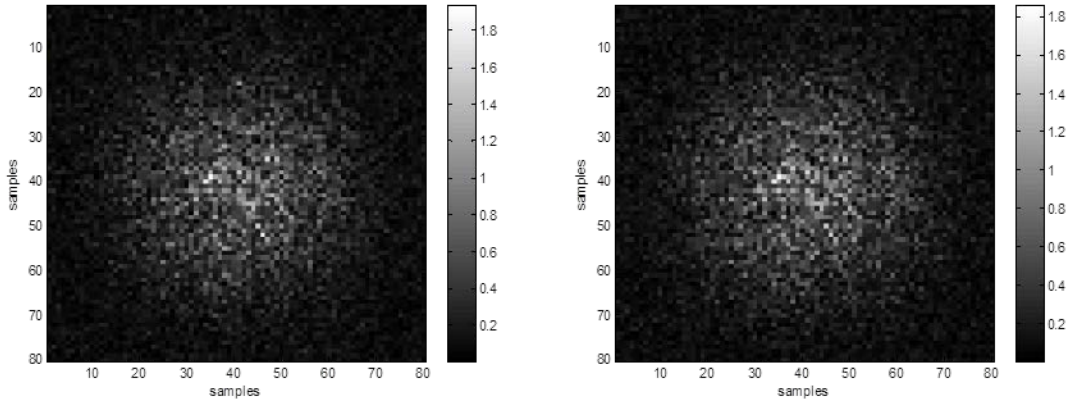


***Figure 22: Cropped Lower Left quadrant of Image Planes***

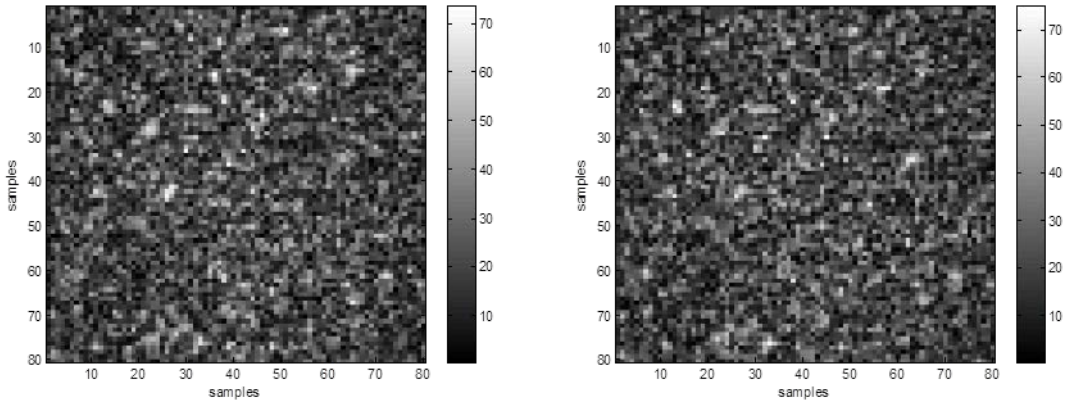


***Figure 23: FT of the Cropped Image Quadrants***

The number of trials was chosen to reduce the fractional uncertainty in the RMS values to less than 2%. For n = 1280 trials the fractional uncertainty of the RMS values is 1.98% (Equation (32)) [31]. More trials can be processed to reduce the uncertainty further but it would be very time consuming. For instance to get a fractional of 1%, 5000 trials would be needed, 4 times as many trials.

$$\text{fractional uncertainty of RMS} = \frac{1}{\sqrt{2(n-1)}} \tag{32}$$

## 3.3 Simulated Results

The results of the simulation are presented in Figure 24. Notice the results are shown on base 10 logarithmic plots to better demonstrate the trends. Recall that the only difference between the simulated frames was the noise that has been added. Therefore all of the data should be zero, however due to the low SNR there are non-zero registration errors.

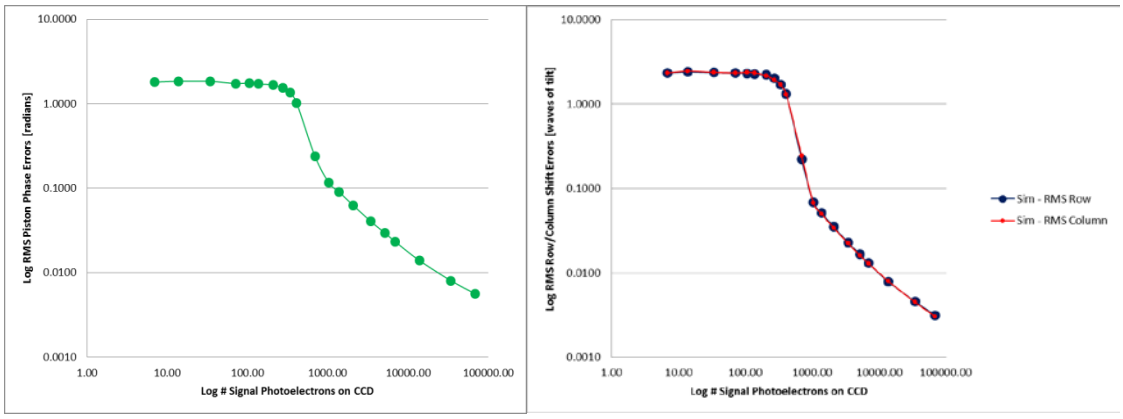


***Figure 24: Simulated Piston Phase (left) and Row and Column Translation (right) Errors as a Function of the Signal Photoelectrons***

For this simulation the signal levels that were tested and the corresponding RMS registration errors are reported in Table 1. These are the same signal levels that were tested in the laboratory experiment. The measurement of the average signal level at the receiver is explained in the next

chapter. Every point in the plots is the RMS of 1280 trials. Each trial has a unique speckle realization. There are three distinct sections of the plots in Figure 24. The first section is nearly linear in the log-log plot and extends from 1,000 total signal photoelectrons on the CCD to higher signal levels. This demonstrates that as the SNR increases the registration errors approach zero. The second section is the transition with a steep slope between about 200 to 1,000 total signal photoelectrons. Finally the third section is the flat line that extends from 0 to about 200 total signal photoelectrons. The second section shows the point at which the registration algorithm breaks down.

***Table 1: Simulated Registration Errors as a Function of Signal Photoelectrons***

| # Signal Photons on the CCD | # Signal Photoelectrons recorded by the CCD | RMS Piston Error | RMS Row Error | RMS Column Error |
|---|---|---|---|---|
| 9.82 | 6.88 | 1.7976 | 2.3326 | 2.3347 |
| 19.54 | 13.68 | 1.8397 | 2.3989 | 2.4581 |
| 48.58 | 34.01 | 1.8362 | 2.3561 | 2.3747 |
| 101.18 | 70.82 | 1.7320 | 2.3344 | 2.3411 |
| 151.03 | 105.72 | 1.7546 | 2.3173 | 2.3675 |
| 196.44 | 137.51 | 1.7091 | 2.2646 | 2.3508 |
| 295.72 | 207.00 | 1.6694 | 2.2107 | 2.1628 |
| 391.83 | 274.28 | 1.5352 | 2.0197 | 1.9245 |
| 485.82 | 340.08 | 1.3596 | 1.7091 | 1.6901 |
| 585.10 | 409.57 | 1.0140 | 1.3194 | 1.2958 |
| 987.49 | 691.24 | 0.2387 | 0.2227 | 0.2450 |
| 1478.59 | 1035.01 | 0.1152 | 0.0686 | 0.0678 |
| 1969.69 | 1378.79 | 0.0902 | 0.0513 | 0.0498 |
| 2978.30 | 2084.81 | 0.0621 | 0.0352 | 0.0342 |
| 4900.47 | 3430.33 | 0.0404 | 0.0228 | 0.0224 |
| 7403.51 | 5182.46 | 0.0293 | 0.0165 | 0.0160 |
| 9927.68 | 6949.38 | 0.0232 | 0.0130 | 0.0129 |
| 19749.74 | 13824.82 | 0.0139 | 0.0078 | 0.0079 |
| 49110.33 | 34377.23 | 0.0080 | 0.0046 | 0.0045 |
| 98748.72 | 69124.11 | 0.0056 | 0.0031 | 0.0030 |

At a signal level less than ~200 photoelectrons the errors are randomly distributed. Below this signal the correlation peak is completely lost in the noise (Figure 25a). For signal levels between 200 and 1,000 photoelectrons, the program cannot always locate the correlation peak among the noise peaks (Figure 25b). Lastly for high signal levels the correlation peak is prominent for every trial (Figure 25c).

The RMS piston phase errors level off at 1.8 radians which is the RMS value of a uniformly distributed random variable ranging between $\pm\pi$. The tilt errors level off at 2.3 waves of tilt

across the CCD which is the RMS value of a uniformly distributed random variable ranging between ±4. When determining the tilt errors, the registration algorithm has been set to only shift the apertures ±4 pixels when looking for correlation peaks. This value was chosen to keep the computational time short. Had the algorithm been set to look for correlation peaks in a larger window it could account for larger relative tilts. However the RMS registration errors as a function of SNR would have the same trend independent of the value at which the errors are random. By limiting the window in which the algorithm searches for the peak, it has been assumed that the apertures are aligned within ±4 waves of tilt over the aperture.

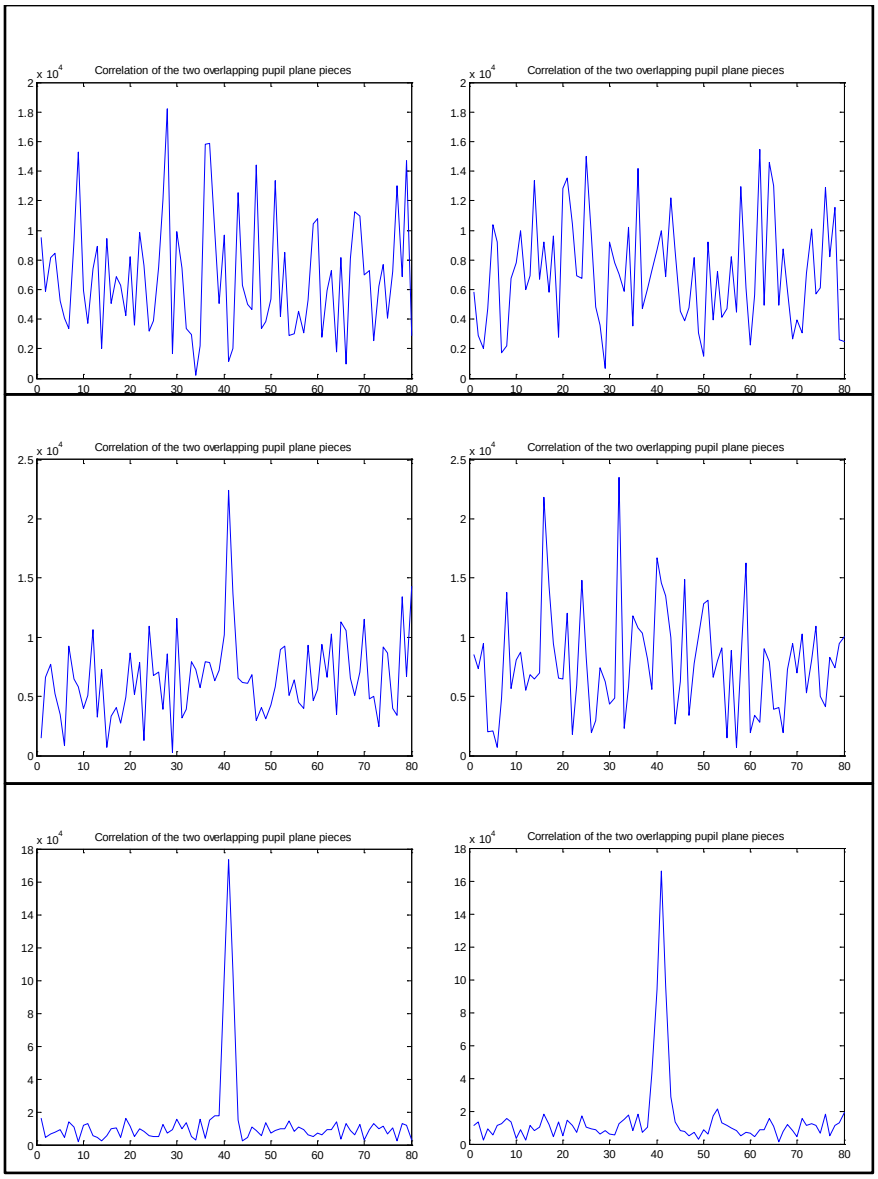


***Figure 25: Plots of Cross-Correlation for Various Numbers of Signal Photoelectrons***

# 4 EXPERIMENT

The experiment was designed to determine how well the registration algorithm could align apertures in perfect conditions with low signal levels. In high signal situations it should be easy to register two images taken of the same target, from the same receiver location. However at low SNR the algorithm can register the noise between frames instead of the signal. The experimental set up described in Chapter 3.1 was designed to capture multiple images in the same location of a single target. The images were taken quickly and processed using the described holographic reconstruction techniques to measure the signal field. The signal field measured from one frame was then registered to the adjacent frame and the errors were recorded. This chapter describes the process for collecting the data and explains the results of the experiment.

## 4.1 Data Collection

The first step to collecting the experimental data was to set the signal level. Measuring signal levels as low as a few hundred photons is very difficult due to noise in the detectors. For this experiment a ratio was determined to relate the transmitted power to the power at the receiver (Equation (33)). This was done using the same set up as Figure 3, except a second Ophir Nova II power detector was put in the place of the CCD camera and the LO path was disconnected. The transmitter power was set using the inline variable attenuator and it was measured with the switch turned to the first power detector. Then the switch was flipped to turn on the TX and the power in the receiver plane was measured by the second power detector. Equation (34) was used to convert the received power over the Nova II into the number of photons that would be incident on the CCD area.

$$\text{Ratio} = \frac{\text{Power at the RX}}{\text{Power from the TX}} \tag{33}$$

$$M = \frac{P_{TX}\,\text{Ratio}\,\frac{A_{CCD}}{A_{Nova}}\,\Delta t}{\frac{hc}{\lambda}} \tag{34}$$

In Equation (34), M is the number of signal photons over the CCD if the transmit power is measured to be $P_{TX}$. The area of the CCD ($A_{CCD}$) is divided by the area of the power detector ($A_{Nova}$) to account for the difference in active detecting area. The power detector had a round area with a diameter of 5 mm, while the CCD was square with a width of 7.7 mm. Next the exposure time, $\Delta t$ was factored in to convert from watts to Joules. Then the energy on the receiver, in Joules, was converted to photons by dividing by the energy per photon for light at wavelength $\lambda$. To convert M into detected photoelectrons, simply multiply by the quantum efficiency of the CCD.

Table 2 contains the power measured at the receiver for a given power set at the transmitter, and the ratio calculated from that data. The average ratio was found to be $4.5\text{x}10^{-6}$. This data was taken with all of the room lights turned off to reduce background noise. In the laboratory the TX was set to a variety of levels, which can be seen in the first column of Table 3. This table calculates the number of signal photons incident on the CCD using Equation (34). The last

column shows the number of signal photoelectrons detected over the CCD. These signal levels were used in the simulation and when plotting the data.

***Table 2: Ratio of the Received and Transmitted Power***

| At TX (filter IN) [mW] | At RX (filter OUT) [nW] | Ratio with Noise Subtracted (RX/TX) |
|---|---|---|
| 1.924 | 8.55 | 4.4335E-06 |
| 1.902 | 8.43 | 4.4217E-06 |
| 1.851 | 8.15 | 4.3922E-06 |
| 1.798 | 7.92 | 4.3938E-06 |
| 1.749 | 7.63 | 4.3511E-06 |
| 1.698 | 7.35 | 4.3168E-06 |
| 1.653 | 7.27 | 4.3860E-06 |
| 1.600 | 6.98 | 4.3500E-06 |
| 1.548 | 6.66 | 4.2894E-06 |
| 1.497 | 6.55 | 4.3621E-06 |
| 1.400 | 6.24 | 4.4429E-06 |
| 1.302 | 5.87 | 4.4931E-06 |
| 1.199 | 5.35 | 4.4454E-06 |
| 1.102 | 4.98 | 4.5009E-06 |
| 1.006 | 4.55 | 4.5030E-06 |
| 0.904 | 4.08 | 4.4912E-06 |
| 0.797 | 3.62 | 4.5169E-06 |
| 0.701 | 3.24 | 4.5934E-06 |
| 0.604 | 2.76 | 4.5364E-06 |
| 0.509 | 2.37 | 4.6169E-06 |
| 0.403 | 1.86 | 4.5658E-06 |
| 0.304 | 1.49 | 4.8355E-06 |
| 0.201 | 1.00 | 4.8756E-06 |
| 0.102 | 0.53 | 4.9608E-06 |

***Table 3: Number of Photoelectrons for Given Transmitter Power***

| Power at TX (W) | Signal at RX (photons) | Signal at RX (photoelectrons) |
|---|---|---|
| 9.30E-10 | 9.82 | 6.88 |
| 1.85E-09 | 19.54 | 13.68 |
| 4.60E-09 | 48.58 | 34.01 |
| 9.58E-09 | 101.18 | 70.82 |
| 1.43E-08 | 151.03 | 105.72 |
| 1.86E-08 | 196.44 | 137.51 |
| 2.80E-08 | 295.72 | 207.00 |
| 3.71E-08 | 391.83 | 274.28 |
| 4.60E-08 | 485.82 | 340.08 |
| 5.54E-08 | 585.10 | 409.57 |
| 9.35E-08 | 987.49 | 691.24 |
| 1.40E-07 | 1478.59 | 1035.01 |
| 1.87E-07 | 1969.69 | 1378.79 |
| 2.82E-07 | 2978.30 | 2084.81 |
| 4.64E-07 | 4900.47 | 3430.33 |
| 7.01E-07 | 7403.51 | 5182.46 |
| 9.40E-07 | 9927.68 | 6949.38 |
| 1.87E-06 | 19749.74 | 13824.82 |
| 4.65E-06 | 49110.33 | 34377.23 |
| 9.35E-06 | 98748.72 | 69124.11 |

There were 10 steps required to collect data for this experiment (Figure 26). The first step was to set the TX level according to the desired levels in Table 3. With all of the room lights turned off, and the LO set to half-well capacity, 128 frames were captured at a time. The LabVIEW program could only save 128 frames worth of data at a time due to memory limitations. Therefore to get enough frames, 10 trials of 128 frames were captured for each signal level. In between each trial of 128 fringe frames, 128 frames of LO only data (TX turned off) were captured. Steps 2 & 3 were repeated 10 times, and then in the laboratory steps 1, 2, and 3 were repeated for all 20 signal levels. An example of a raw fringe data for a signal level of 100,000 received photons, and a LO only frame can be seen in Figures 27 & 28.

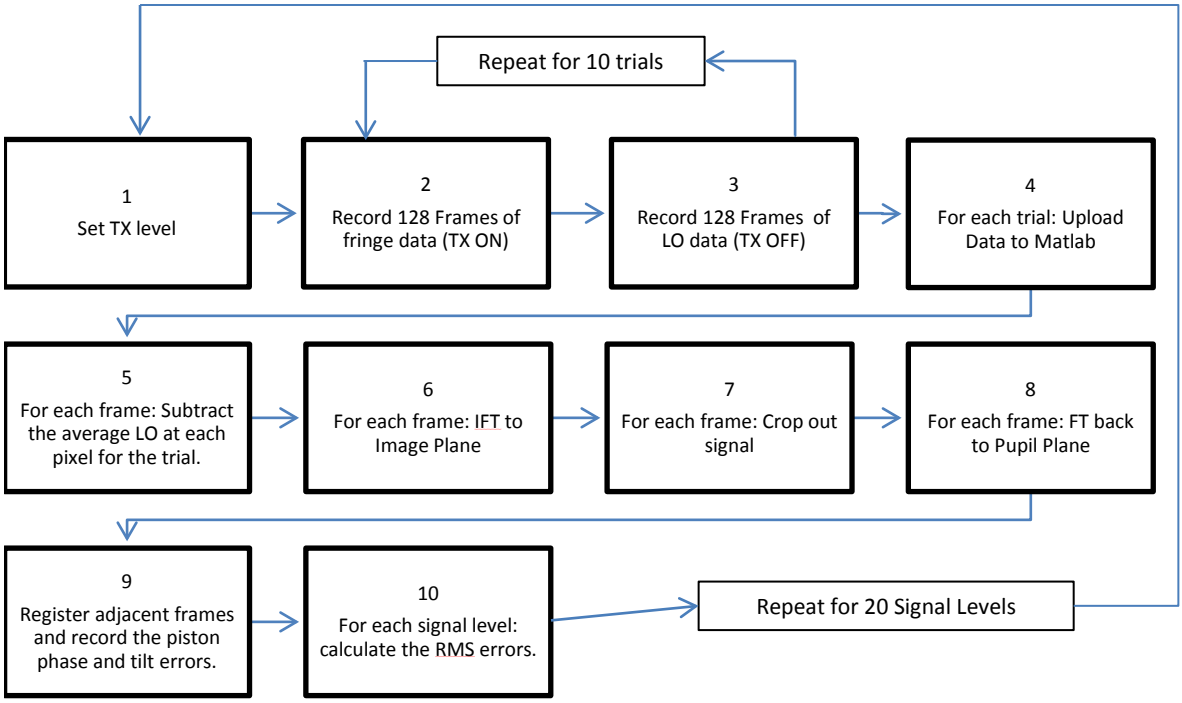


***Figure 26: Flowchart for Collecting and Processing Data***

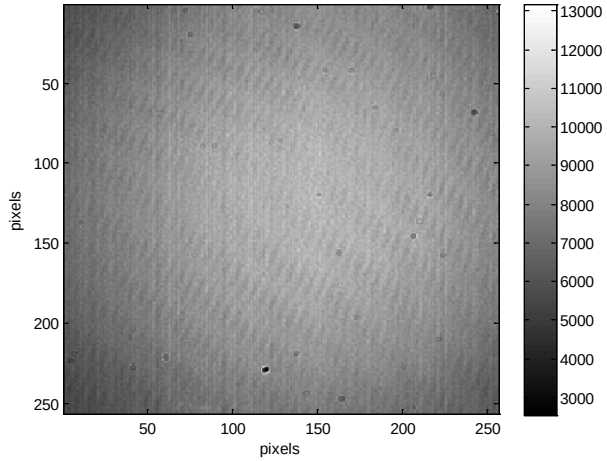


***Figure 27: Raw Signal Plus LO Data for 69,125 Photoelectrons***

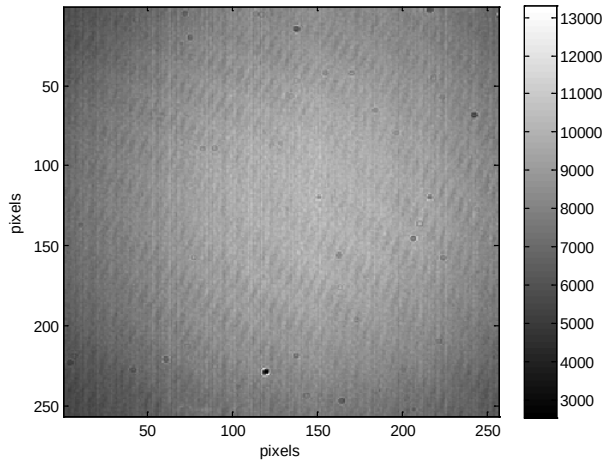


***Figure 28: Raw LO Only Data at Half Well Capacity***

## 4.2 Data Processing

Once all of the data was collected it was uploaded into Matlab, one signal level at a time. For each trial the average LO value at each pixel was calculated (Figure 29). Step 5 was to subtract this average from each fringe frame in the trial to remove any static background noise (Figure 30). This background noise includes any camera noise or extra light sources that are stationary over all of the frames.

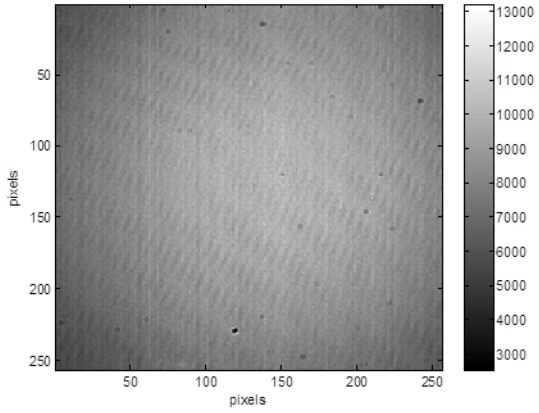


***Figure 29: Average LO Over 128 Frames***

Next for each frame the inverse Fourier Transform was used to propagate the data to the image plane (Figure 31). From there the signal field was extracted by cropping out the lower left quadrant (Figure 32). Step 8 was to Fourier Transform the signal field back to the pupil plane for each aperture (Figure 33). The adjacent frames were then plugged into the speckle cross-correlation algorithm. These frames were already aligned in the laboratory, such that the output from the algorithm should be zero. Any non-zero outputs were errors due to individual noise on each frame. For each signal level the RMS piston phase and tilt errors were calculated and plotted. Then steps 4-10 were repeated for the 20 signal levels.

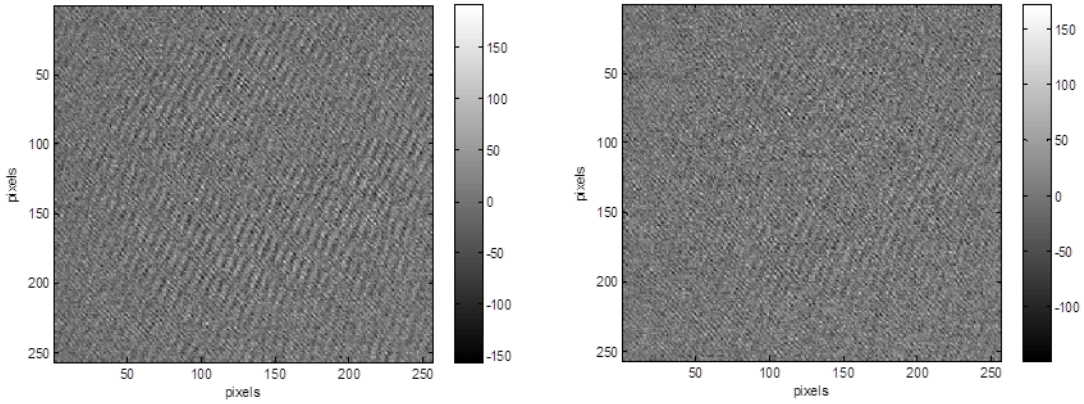


***Figure 30: Two Frames of Signal Mixed with LO after Background Subtraction***

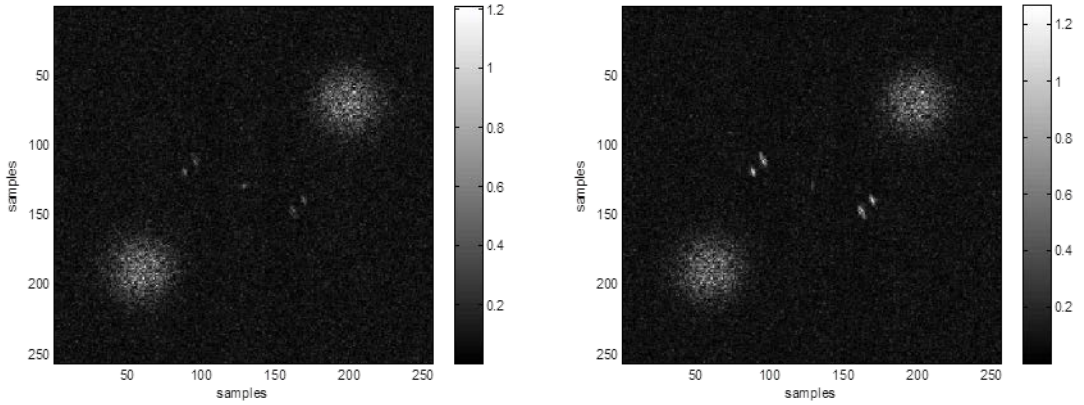


***Figure 31: Images from Each Frame (IFT of the Fringes)***

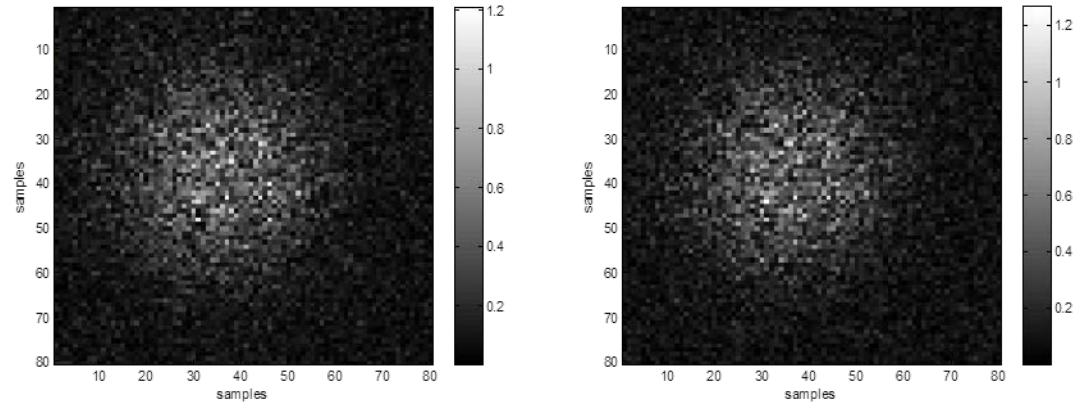


***Figure 32: Cropped Lower Left Quadrant of Each Image***

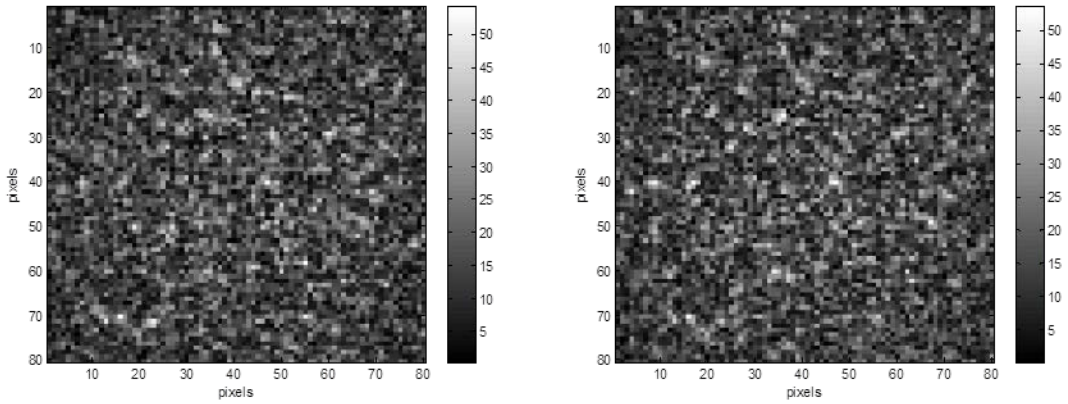


***Figure 33: FT of Cropped Images***

## 4.3 Experimental Results

The experimental RMS registration errors as a function of received signal level are presented on logarithm plots in Figure 34. They can also be seen in Table 4. Notice these plots approach zero at high signal levels and plateau at 1.8 radians for the piston phase and 2.3 waves of tilt over the CCD for the tilt errors. Recall that these errors represent the RMS of a uniformly distributed random variable over [-π, π] radians and [-4, 4] pixels, respectively. The plots can be interpreted such that at received signals below about 200 photoelectrons across the entire CCD the speckle registration program will randomly register the apertures due to the random shot noise overwhelming the signal.

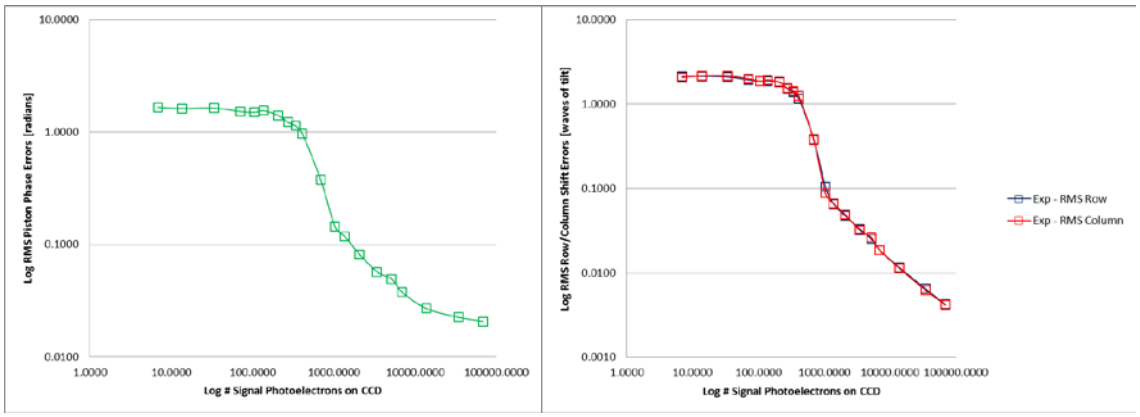


***Figure 34: Experimental Piston Phase (Left) and Row and Column Translation (Right) Errors as a Function of Signal Photoelectrons***

***Table 4: Experimental Registration Errors for Various Signal Photoelectrons***

| # Signal Photons on the CCD | # Signal Photoelectrons recorded by the CCD | RMS Piston Error | RMS Row Error | RMS Column Error |
|---|---|---|---|---|
| 9.8221 | 6.8754 | 1.6580 | 2.1124 | 2.0727 |
| 19.5385 | 13.6770 | 1.6220 | 2.1406 | 2.1646 |
| 48.5823 | 34.0076 | 1.6355 | 2.1025 | 2.1633 |
| 101.1778 | 70.8245 | 1.5267 | 1.9341 | 2.0071 |
| 151.0275 | 105.7192 | 1.4991 | 1.8688 | 1.8683 |
| 196.4413 | 137.5089 | 1.5499 | 1.8780 | 1.9443 |
| 295.7181 | 207.0027 | 1.4057 | 1.8280 | 1.8167 |
| 391.8265 | 274.2785 | 1.2210 | 1.5136 | 1.5518 |
| 485.8226 | 340.0758 | 1.1369 | 1.3744 | 1.4258 |
| 585.0994 | 409.5696 | 0.9702 | 1.1679 | 1.2487 |
| 987.4872 | 691.2411 | 0.3772 | 0.3808 | 0.3730 |
| 1478.5905 | 1035.0133 | 0.1445 | 0.1049 | 0.0877 |
| 1969.6938 | 1378.7856 | 0.1174 | 0.0654 | 0.0663 |
| 2978.3037 | 2084.8126 | 0.0815 | 0.0473 | 0.0489 |
| 4900.4713 | 3430.3299 | 0.0570 | 0.0331 | 0.0319 |
| 7403.5138 | 5182.4597 | 0.0493 | 0.0251 | 0.0261 |
| 9927.6790 | 6949.3753 | 0.0376 | 0.0185 | 0.0185 |
| 19749.7443 | 13824.8210 | 0.0269 | 0.0115 | 0.0113 |
| 49110.3268 | 34377.2288 | 0.0225 | 0.0064 | 0.0062 |
| 98748.7217 | 69124.1052 | 0.0206 | 0.0042 | 0.0041 |

The experimental data can be analyzed in four sections. At the highest signal levels the RMS piston phase plot approaches 0.02 radians, instead of zero as expected. This can be understood by considering how much the target would have to move relative to the RX to induce 0.02 radians of phase noise into the system. Equation (35) can be used to calculate the physical distance, $\Delta R$, between frames that corresponds to 0.02 radians of extra phase. For a wavelength of 1545 nm, the range would have to vary 5 nm on average between frames.

$$\Delta R = \frac{\lambda}{2\pi}\Delta\phi = \frac{1545\text{ nm}}{2\pi}(0.02\text{ rad}) = 5\text{ nm} \tag{35}$$

The time between frames is the inverse of the frame rate, 120 Hz, or 8.33 milliseconds.

Therefore the velocity of the relative motion in the system, v, would have to be on average 0.6 μm/s (Equation (36)). This velocity is small enough to be reasonable. It can be expected that the experimental system will vibrate, especially if the optical table is not floating. This extra phase noise means that even at high signal level, once the registration algorithm has overcome the shot noise, it is still limited by the vibrations in the system.

$$v = \frac{\Delta R}{\Delta T} = \frac{5\text{ nm}}{8.33\text{ ms}} = 0.6\frac{\mu m}{s} \tag{36}$$

This effect can be seen on the piston phase plot is because piston is sensitive to longitudinal motions on the order of the wavelength, 1545 nm. The tilt errors on the other hand are sensitive to transverse motion on the order of the speckle size at the target. The speckle size at the target is 400 μm (Equation (37)). This is much larger than the wavelength. Therefore there should be a similar non-zero limit that the RMS tilt errors approach, but it will be at a much lower RMS tilt error value than that of the piston. Conversely, it should appear at much higher signal.

$$D_{speckle} = \frac{\lambda z}{D_{CCD}} = \frac{1545\text{ nm} * 2\text{ m}}{7.7\text{ mm}} = 400\ \mu m \tag{37}$$

Figure 35 shows the experimental results compared to the simulated results. Notice these lines are nearly matched which suggests that the simulation has accounted for a majority of the noise, or that the experiment is shot noise limited. However the trend lines are not exactly the same. The slope of the high signal section is similar for all four lines. However the simulation is shifted by a factor of ~1.6 away from the experimental data. This factor could be explained by a few different physical aspects of the experiment that were not modeled. For instance in the simulation the amount of the signal field that mixes with the LO field, or the mixing efficiency, was nearly 100%. However in the laboratory, any variations in the polarization, or if the quantum efficiency is not constant over the CCD, or if there is pixel cross talk or any decrease the mixing efficiency between the coherent beams will shift the data.

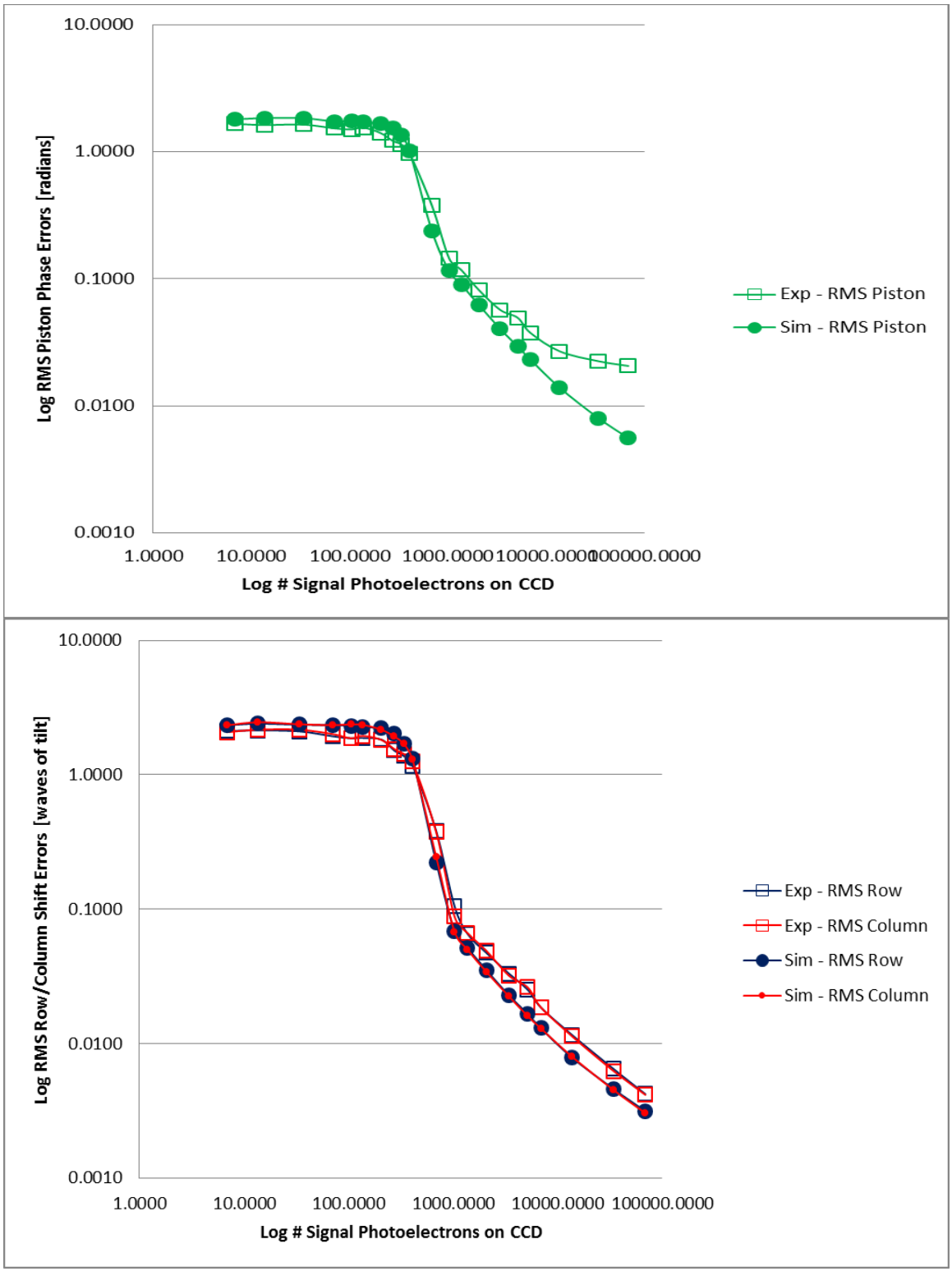


***Figure 35: Experimental vs. Simulated Piston Phase (Top) and Row and Column Translation (Bottom) Errors***

Also notice that the slope of the transition section and the point where the low signal section begins for the simulation does not match the experimental data. This can be explained by

considering that if there are any extra photons hitting the CCD in the laboratory they would only affect the low signal errors on these plots. Since these are logarithmic plots, a few hundred extra photons would not change the shape of the trend at high signal, but would shift where the transition happens at lower signals. These extra photons in the laboratory, which were not simulated in the model, could have scattered off of any reflective surface in the room. The extra photons must be time varying at a rate that is faster than the time between frames, but slower than the time between trials. Otherwise they would have been subtracted out as background noise.

The highest probability is that some of the incoming signal reflected off of the cover glass on the CCD before being detected. Figure 36 shows the image plane for an aperture from the simulation on the left, and from the experiment on the right. These images are both from a high signal situation so that the signal can be seen over the noise floor. Notice on the experimental data there are two sets of two bright spots diagonally above and below the zeroth order information. There is a good chance that these bright spots are due to the light reflecting off the CCD and then the front and back of the cover glass as demonstrated in Figure 37.

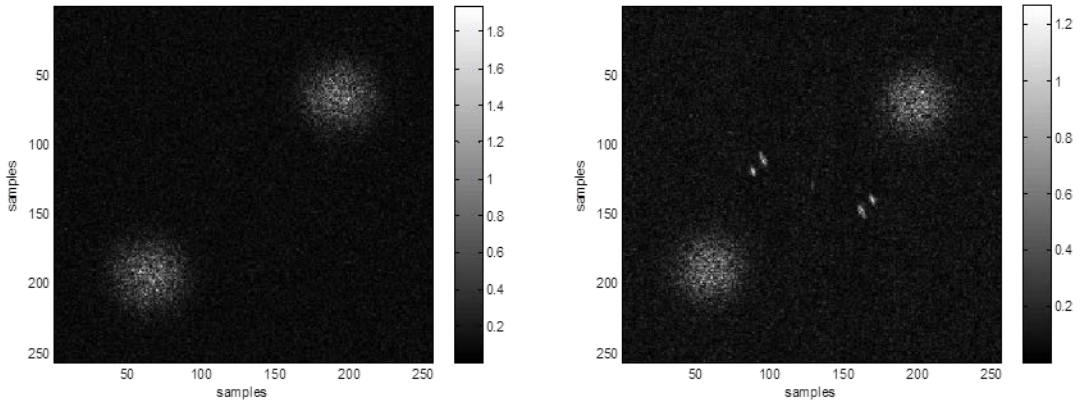


***Figure 36: Experimental vs. Simulated Images***

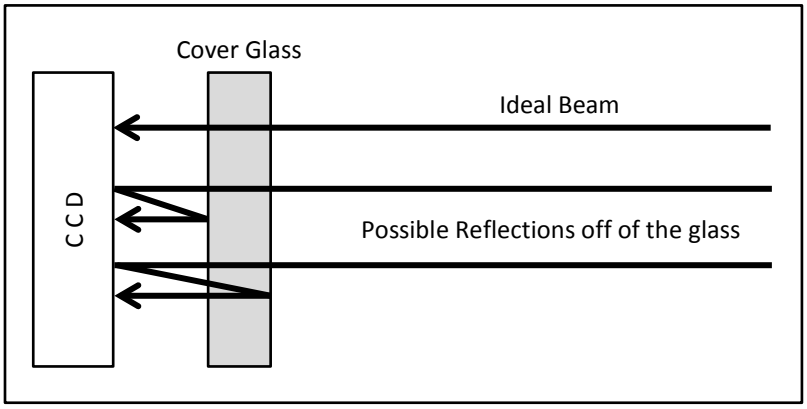


***Figure 37: Possible Paths through the Cover Glass to the CCD***

# 5 REGISTRATION ERROR EFFECTS ON IMAGE QUALITY

The second part of the simulation investigates the effect of the registration errors on the modulation transfer function (MTF). The model will plot the MTF for a synthetic aperture made up of two overlapping apertures assuming that the registration program has not accurately aligned the sub-apertures. The errors will be set using the simulated and experimental results. Also the effect of these errors on larger synthetic apertures will be demonstrated. The final section of this chapter will examine how the errors affect the MTF if they are compounded over many sub-apertures to create a larger synthetic aperture.

## 5.1 MTF of a Synthetic Aperture with Two Sub-Apertures

When modeling the effects of the registration errors on the MTF, a point target was chosen to capture all of the spatial frequency information at once. In the far field the response from a point target appears flat. Therefore the model starts by creating an array of ones in the pupil plane. In this model all of the apertures are overlapped by half an aperture diameter. Consider for now, that there are only two overlapping apertures. Each aperture captures an image of the flat pupil field. The first aperture will be the reference frame with an initial piston phase and tilt of zero. The piston phase, tip and tilt errors on the second aperture are applied according to the errors found in the laboratory. The programming steps that were used are summarized in Figure 38.

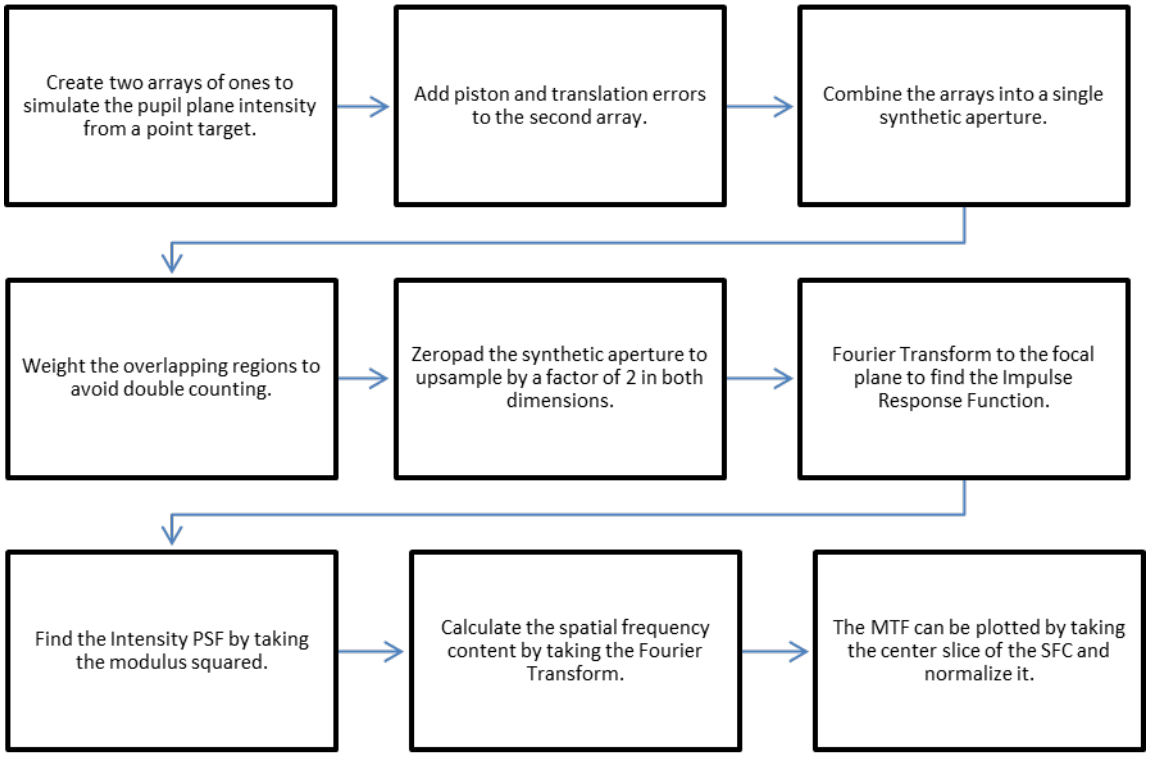


***Figure 38: Flowchart for Modeling Effects of Registration Errors on the MTF***

$$(\text{Aperture})_n = A_0 \exp[jp_n + j\pi r_n \left(\frac{D}{\Delta x}\right) x + j\pi c_n \left(\frac{D}{\Delta y}\right) y \qquad (38)$$

Equation (38) demonstrates how the piston phase, tip and tilt errors are added to the second aperture. The amplitude $A_0$ is simply an array of ones, the same size as the number of speckles

across one aperture. The number of speckles across one dimension of the receive aperture is equal to the number of resolution cells in one dimension of the image. The number of speckles can be found by dividing the image size by the spot size (Equation (39)). The image size in the focal or image plane can be found by multiplying the magnification, f/z, by the object diameter, $D_{obj}$. Here f is the focal length of the lens in the pupil plane and z is the propagation distance between the object and the pupil plane. For this system a digital lens is used, therefore f = z, and the magnification is equal to 1. The spot size in the image plane is equal to the wavelength, λ, multiplied by z, and divided by the aperture diameter, $D_{ap}$. For a 7.7 mm square receive aperture, a 20 mm target, with a wavelength of 1.545 μm, and a range of 2 m, there are 50 speckles across one dimension.

$$\#\ of\ speckles = \frac{Image\ Size\ at\ Image\ Plane}{Spot\ Size\ at\ Image\ Plane} = \frac{\frac{f}{z}D_{obj}}{\frac{\lambda z}{D_{ap}}} = \frac{D_{ap}D_{obj}}{\lambda z} \tag{39}$$

The errors $\{p_n, r_n, c_n\}$ are all weighted by the experimental RMS error results, {p, r, c}. For now, the worst case will be used with an RMS piston phase error of p = 0.1445 radians, r = 0.1049 waves of tilt over the CCD in the x dimension (row dimension), and c = 0.0877 waves of tilt over the CCD in the y dimension (column dimension). These results were found in the laboratory for a signal of 1035 photoelectrons over the CCD. This case was chosen because it had the most severe errors while still being able to find the correlation peak over the noise. These errors will have the maximum effect on the MTF. The specific errors applied to the aperture, $\{p_n, r_n, c_n\}$, are found by multiplying the RMS errors, listed above, by a random number with a Gaussian distribution between zero and one.

Once the two apertures have been created with relative errors between them, they are combined into a synthetic aperture. The overlapping section is multiplied by 0.5 to weight the amplitude to avoid double counting. An example of the absolute value of the synthetic aperture for two apertures, overlapped by half an aperture, can be seen in Figure 39. Next the synthetic aperture array is inserted into an array of zeros (zero-padded) that is twice as large in both dimensions (Figure 40).

When the aperture is Fourier Transformed, to produce the Impulse Response Function, the array will be effectively up-sampled by a factor of 2 (Figure 41). The Intensity Point Spread Function (PSF) is found by taking the modulus squared of the Impulse Response Function (Figure 42). The spatial frequency content can then be plotted by taking the Fourier Transform of the PSF (Figure 43). The MTF is the normalized central strip of the spatial frequency content. Figure # 44 shows the MTF for the two apertures combined into a synthetic aperture with the relative phase errors applied to the second aperture. Only the positive spatial frequencies are plotted. The plot also has the theoretical MTF, which matches the experimental MTF almost exactly. According to the model, the MTF is not significantly affected by the registration errors caused by shot noise when there are two apertures overlapped by half a diameter.

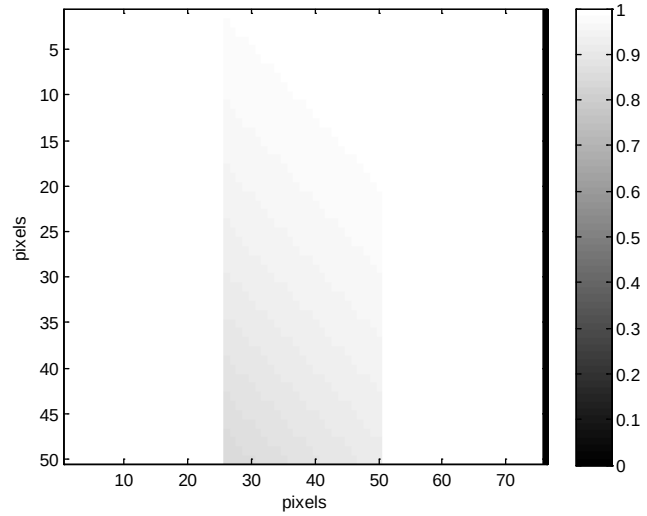


***Figure 39: Image of the Absolute Value of Two Apertures Added Together***

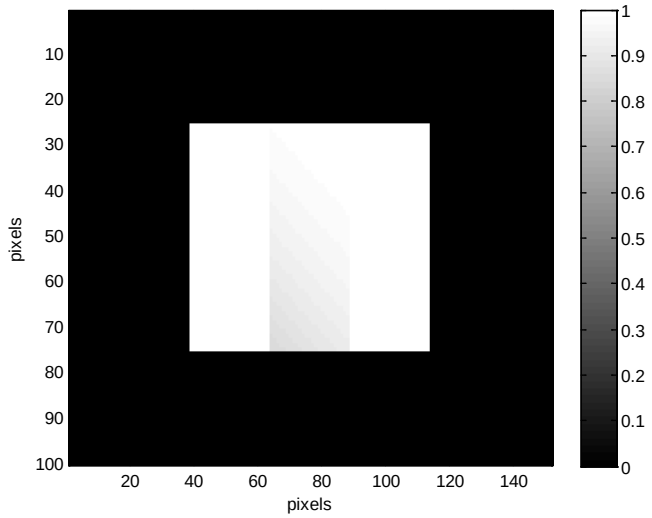


***Figure 40: Synthetic Aperture Embedded in an Array of Zeroes***

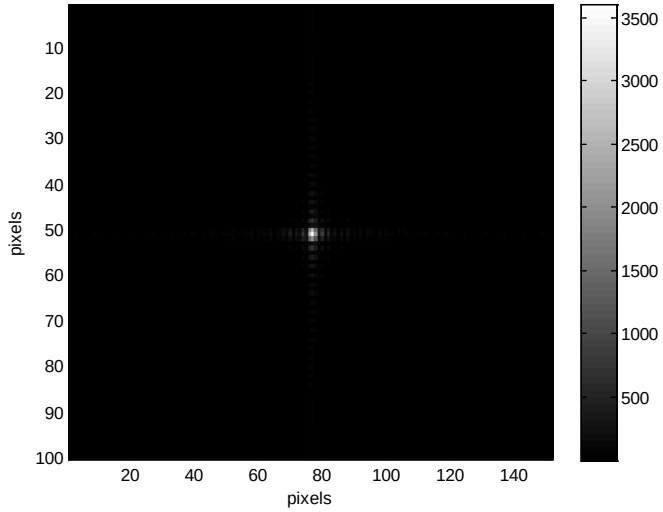


***Figure 41: Impulse Response Function with Relative Piston and Tilt Errors***

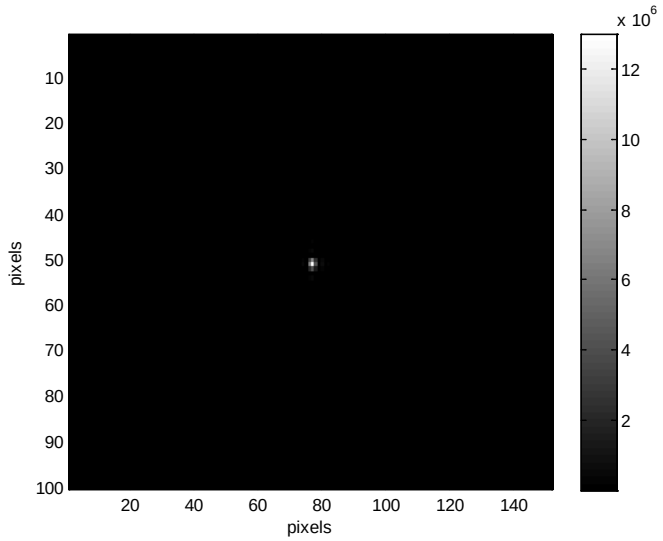


***Figure 42: Intensity Point Spread Function with Relative Piston and Tilt Errors***

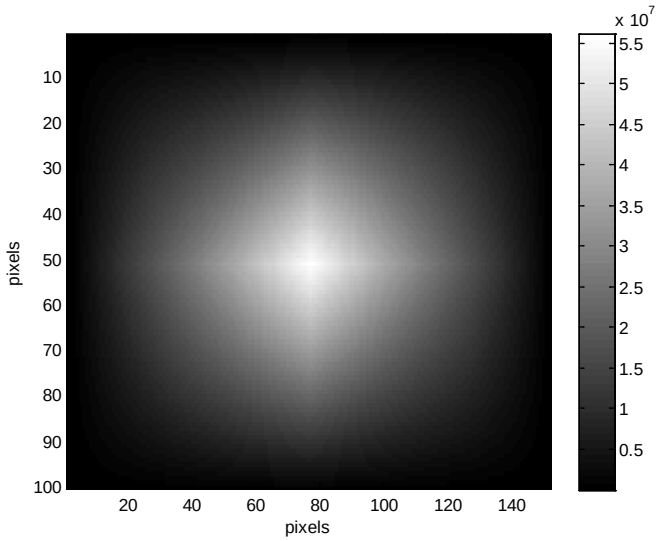


***Figure 43: Spatial Frequency Content with Relative Piston and Tilt Errors***

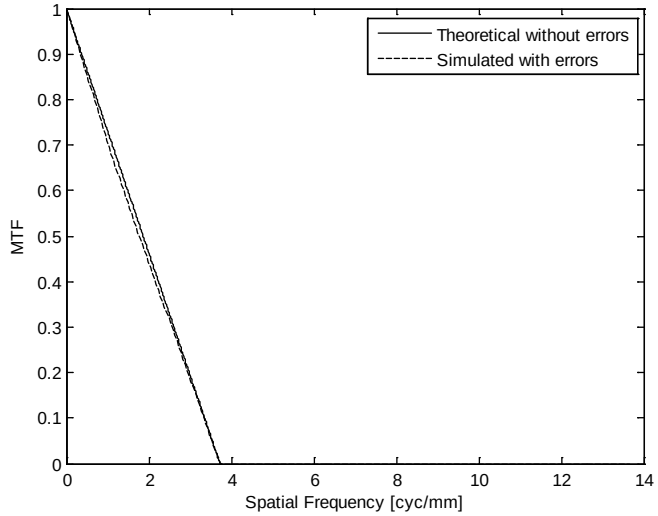


***Figure 44: Average MTF Over 100 Trials with Relative Piston and Tilt Errors***

## 5.2 MTF of a Synthetic Aperture with Multiple Sub-Apertures

Next consider a synthetic aperture made of more sub-apertures. In this case the registration errors will randomly misalign each of the sub-apertures, effectively compounding the errors. The errors applied to each aperture were calculated using Equations (40), (41) & (42). The phase and tilt errors added to the apertures are $\{p_n, r_n, c_n\}$ and the difference between the errors of each aperture are $\{p_{nm}, r_{nm}, c_{nm}\}$. The differences between each aperture are found by multiplying the RMS errors, p, r & c, by a zero mean random number from a normal distribution.

$$p_n = p_{n-1} + \pi c_{(n-2)(n-1)} + p_{(n-1)n} + \pi c_{(n-1)n} \tag{40}$$

$$r_n = r_{n-1} + r_{(n-1)n} \tag{41}$$

$$c_n = c_{n-1} + c_{(n-1)n} \tag{42}$$

Figure 45 describes how the errors and differences between each aperture are defined. The first aperture has no errors applied therefore, $p_1 = r_1 = c_1 = 0$. All of the relative phase shifts are applied to each aperture at the center of the aperture. However they are defined in terms of the center of the overlap region or the part that was registered. To redefine the phase shifts in terms of the center of the aperture the column pixel shifts need to be added. Therefore for the second aperture the piston phase error of the first aperture is added to the difference in phase, $p_{12}$, and $\pi$ times the difference in the column errors over half of the aperture, $c_{12}/2$. The tilt errors are defined in terms of waves of tilt over the entire aperture. To find the compounded tilt errors, simply add the change in row and column shifts from the previous apertures (Equations (41) & (42)).

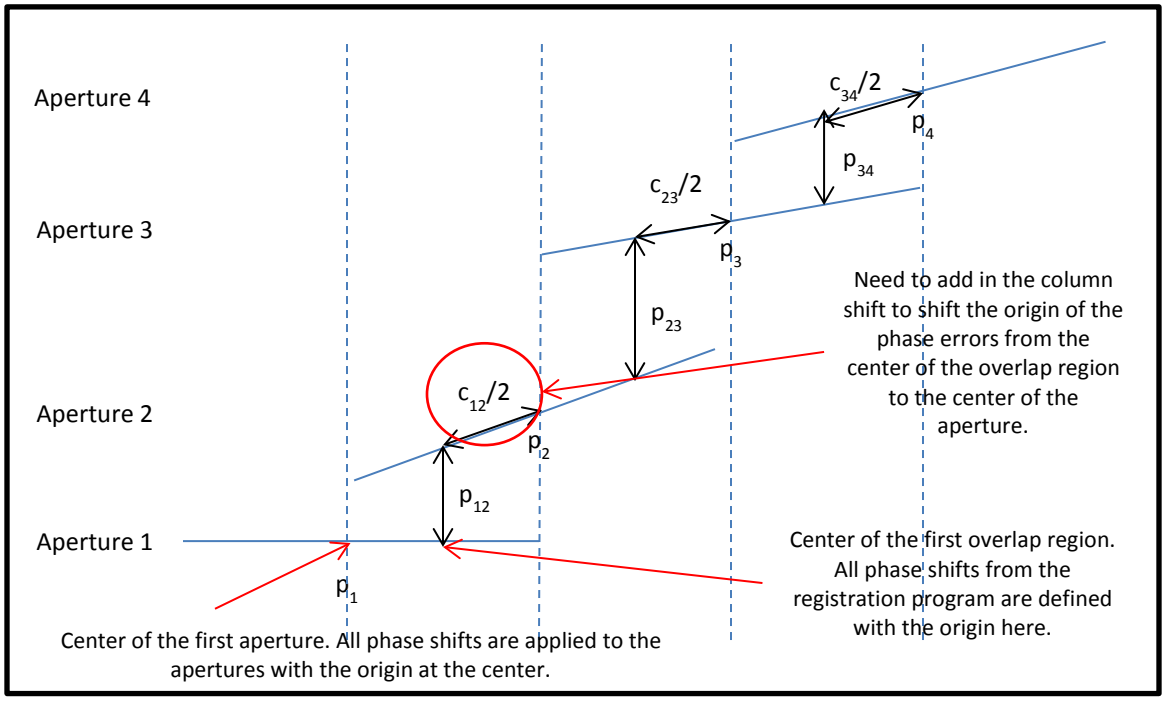


***Figure 45: Diagram Explaining the Relative Errors between Multiple Apertures***

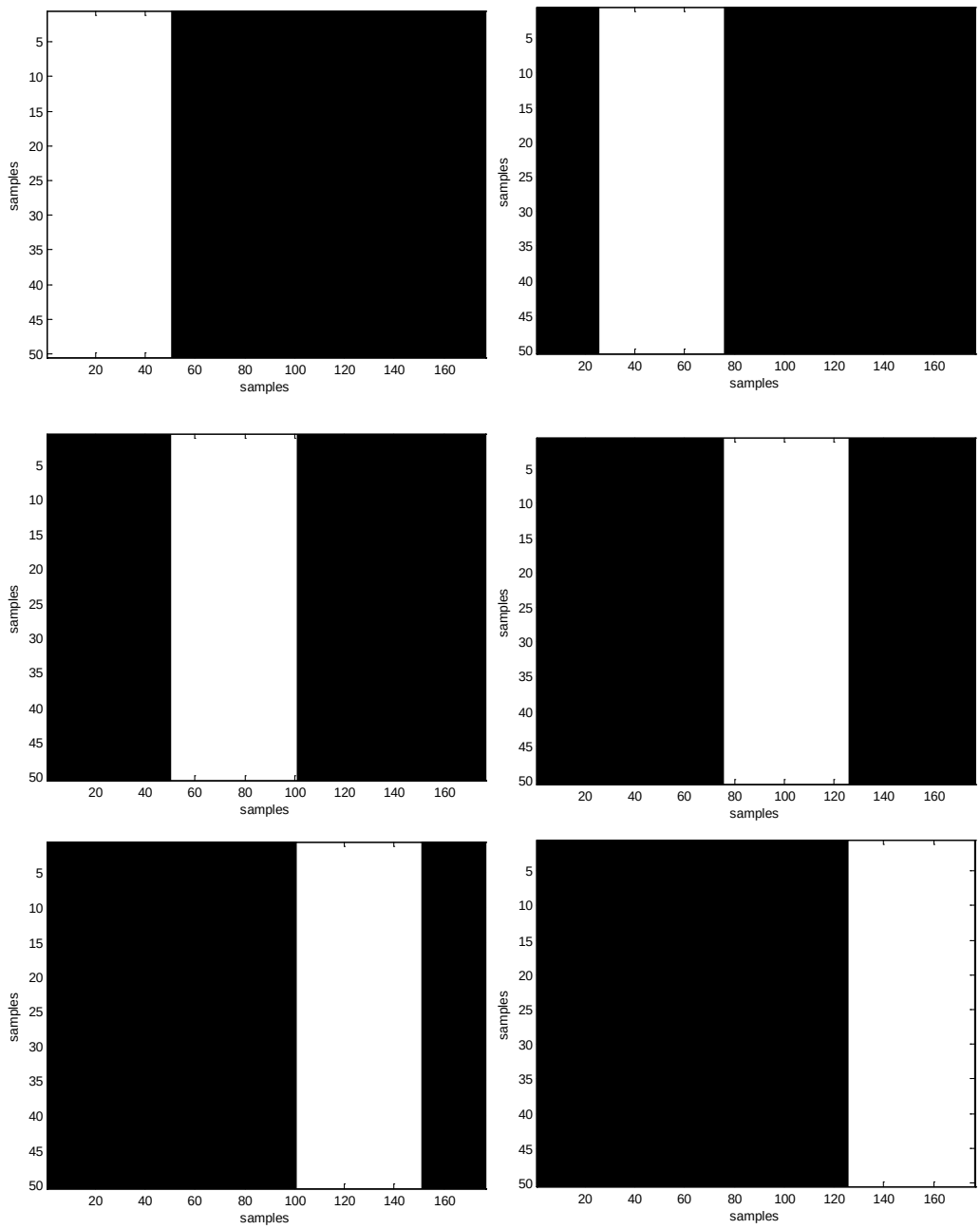


***Figure 46: Absolute Value of Example Sub-Apertures of a Synthetic Aperture***

Consider an example synthetic aperture made up of 6 sub-apertures. Figure 46 shows the six simulated apertures. Each of the images is the absolute value of the aperture therefore the phase errors cannot be seen. The apertures are combined into a synthetic aperture in Figure 47. Once again this is the absolute value, but now the phase differences can be seen as variances in the amplitude. The amplitude of the overlapped regions is weighted by 0.5 to avoid double counting (Figure 48). Next the synthetic aperture is zero-padded (Figure 49), and consequentially up-sampled when Fourier Transformed to find the Impulse Response Function (Figure 50). The Intensity PSF is the modulus squared of the Impulse Response Function (Figure 51). Figure 52 shows the spatial frequency content, which is used to plot the MTF (Figure 53). This process was repeated for 100 trials with individual realizations of the compounded errors, and then averaged.

The final MTF for 6 sub-apertures can be seen in Figure 56. Only the positive spatial frequencies are plotted.

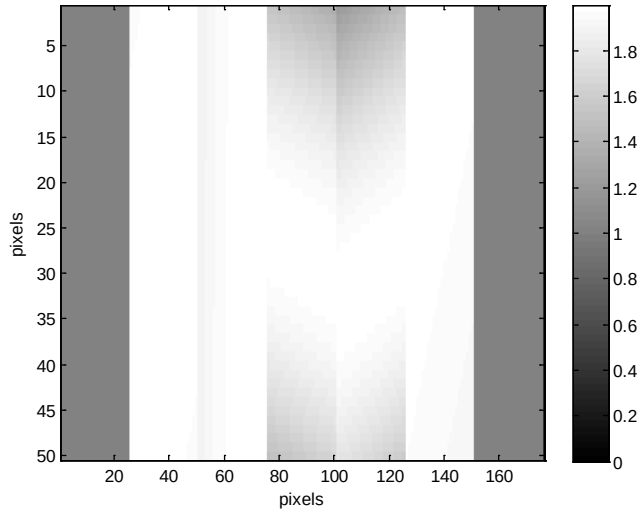


***Figure 47: Absolute Value of the Synthetic Aperture with Compounded Errors***

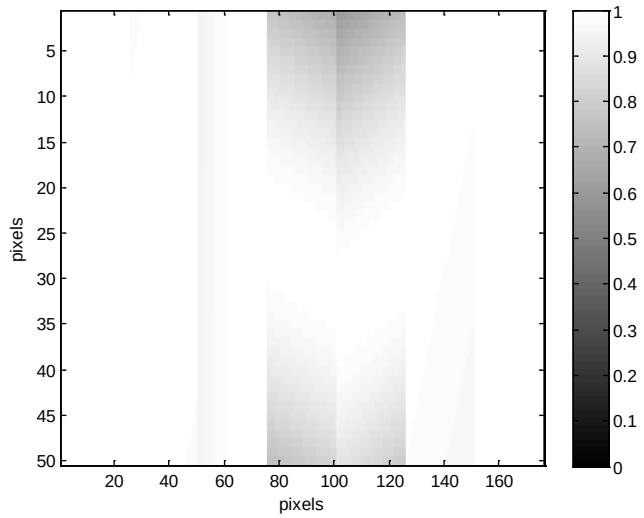


***Figure 48: Synthetic Aperture with Normalized Overlapping Regions***

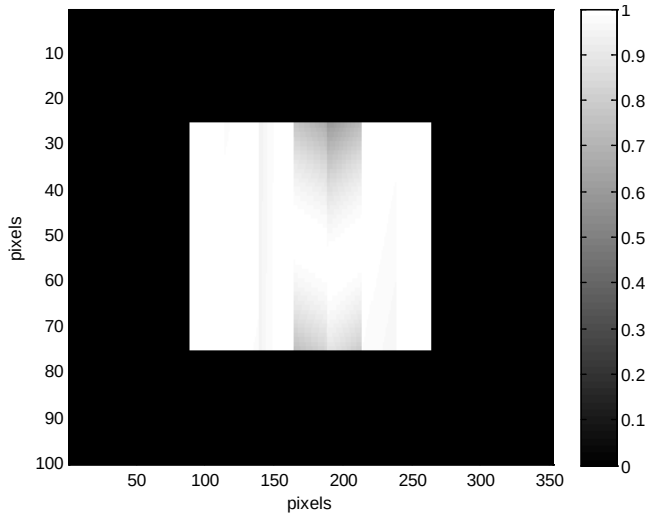


***Figure 49: Synthetic Aperture Embedded in an Array of Zeroes***

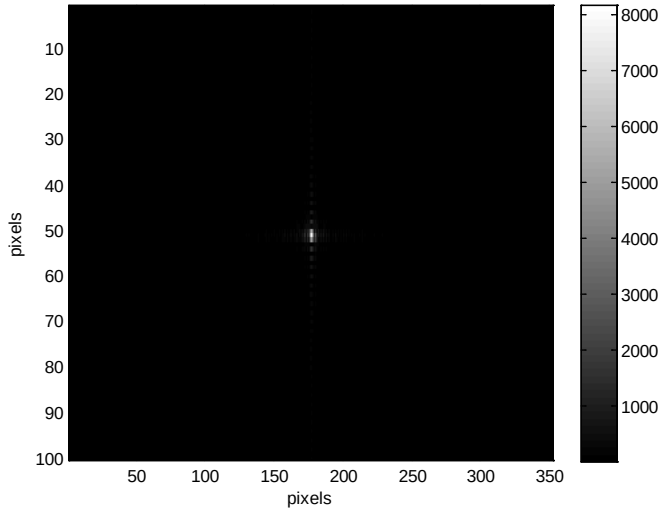


***Figure 50: Impulse Response Function with Sub-Aperture Piston and Tilt Errors***

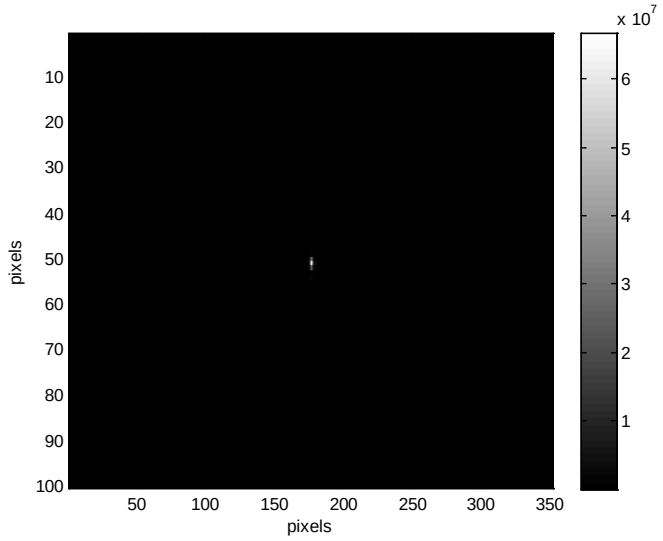


***Figure 51: Intensity Point Spread Function with Sub-Aperture Piston and Tilt Errors***

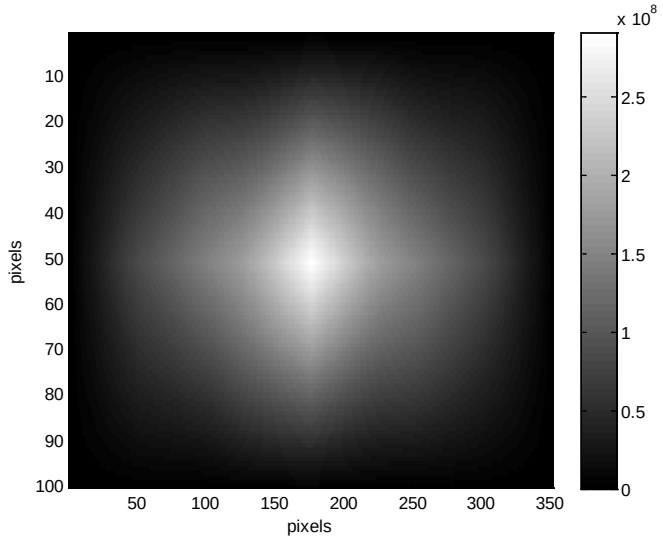


***Figure 52: Spatial Frequency Content with Sub-Aperture Piston and Tilt Errors***

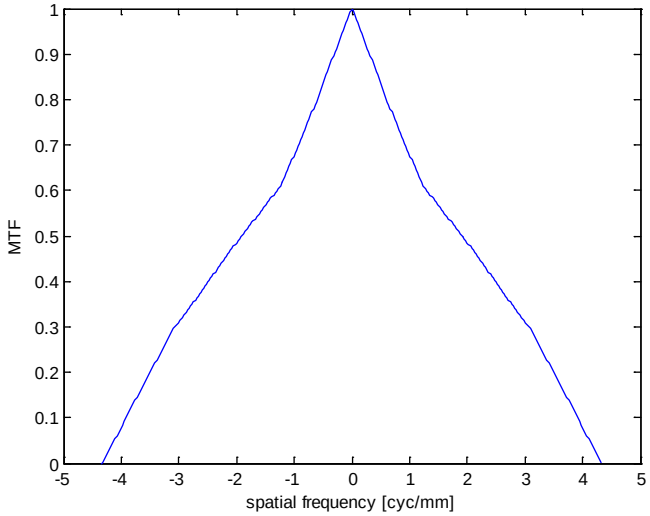


***Figure 53: MTF with Sub-Aperture Piston and Tilt Errors***

Figures 54-58 show the MTF for 2, 4, 6, 8 and 10 sub-apertures. The solid lines are the theoretical MTF plots, according to the spatial frequency bandwidth (Equation (27)). The dashed line shows the simulated MTF where the apertures are aligned except for compounded registration errors due to shot noise. Notice that the errors found from the experiment do not significantly affect a synthetic aperture made up of 2 sub-apertures. However as the number of sub-apertures increases, the compounded errors have a more drastic effect on the mid-range spatial frequencies of the MTF. Figure 59 shows all of the MTF plots with increasing number of sub-apertures for direct comparison. As the apertures are stitched together there is apparent defocus across the synthetic aperture due to the apertures not being properly aligned [20].

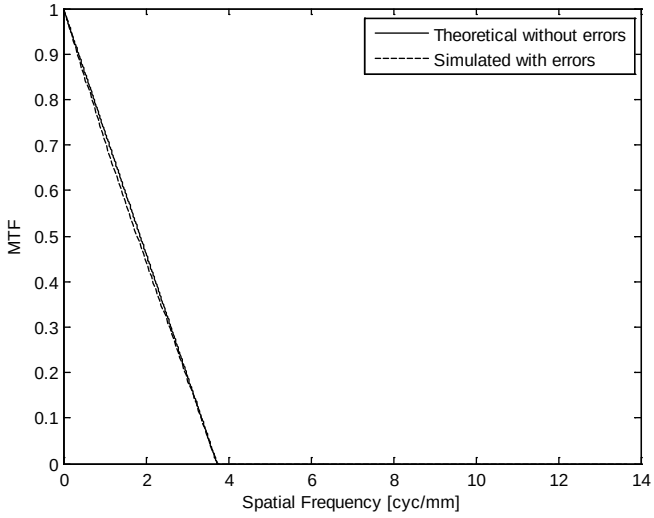


***Figure 54: Average MTF Over 100 Trials for 2 Sub-Apertures***

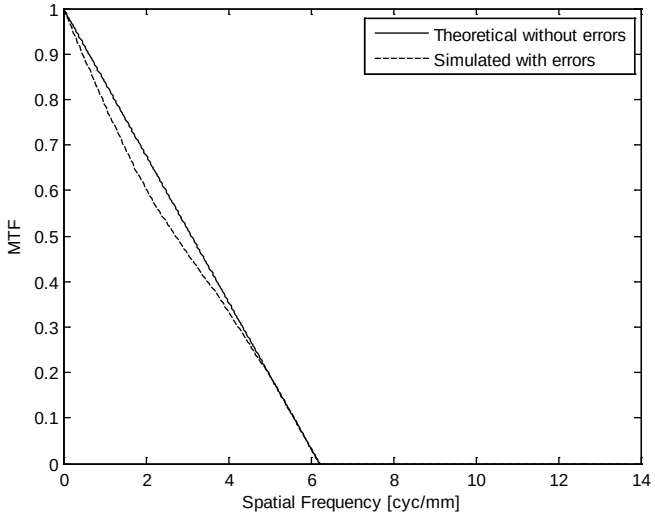


***Figure 55: Average MTF Over 100 Trials for 4 Sub-Apertures***

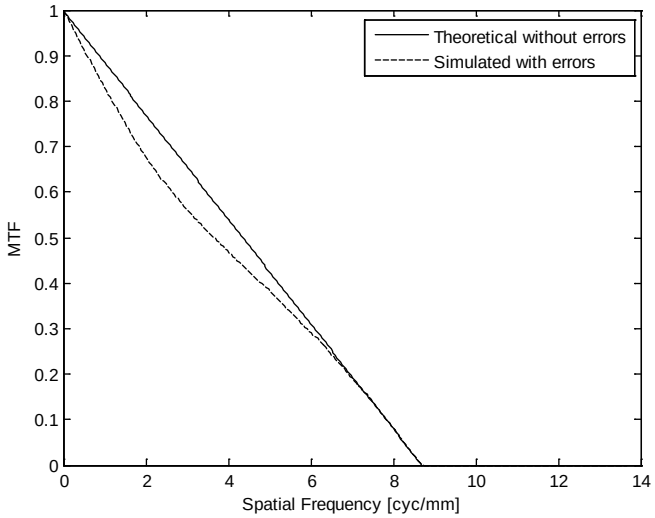


***Figure 56: Average MTF Over 100 Trials for 6 Sub-Apertures***

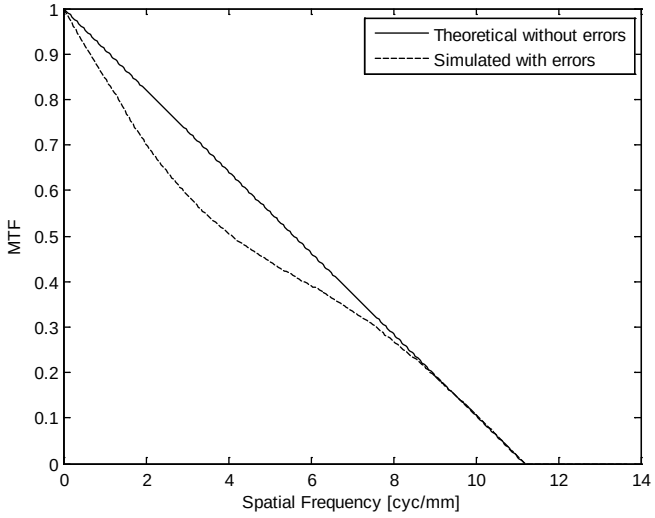


***Figure 57: Average MTF Over 100 Trials for 8 Sub-Apertures***

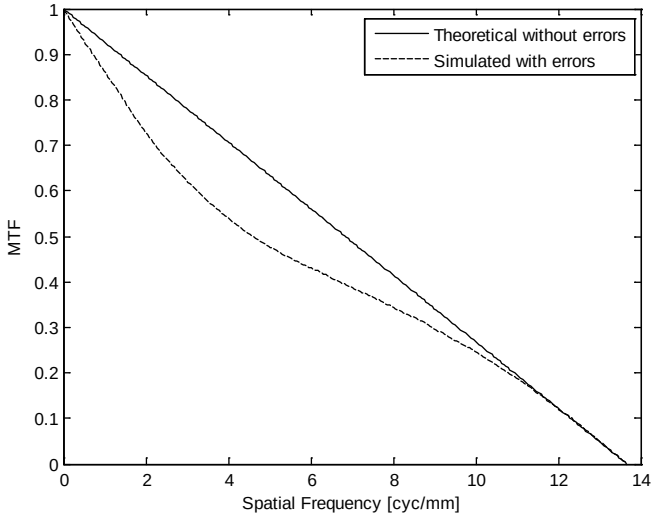


***Figure 58: Average MTF Over 100 Trials for 10 Sub-Apertures***

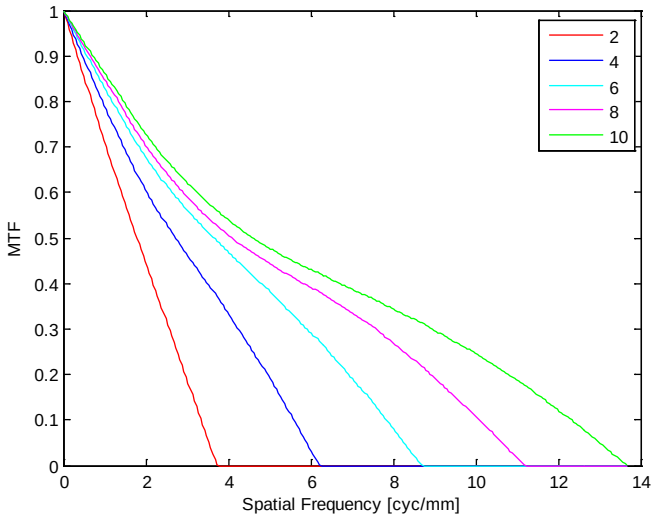


***Figure 59: Average MTF Over 100 Trials for Various Numbers of Sub-Apertures***

# 6 CONCLUSION

## 6.1 Summary of Findings

The goal of this work was to examine the effect of low signal on the registration process used to align overlapping sub-apertures. For this work a shot noise limited bi-static heterodyne coherent ladar detection system was used. Multiple frames with independent shot noise were captured in the laboratory and simulated using Matlab. These frames were processed using digital holographic techniques to extract the signal field. The signal fields from multiple overlapping sub-shots were then registered using an efficient speckle cross-correlation algorithm with sub-pixel accuracy.

The results from the simulation and the experiment were very similar. The RMS registration errors recorded were the piston phase errors, and tilt errors in the form of translations in the image plane. The apertures were perfectly aligned in the laboratory and the model, therefore any registration errors were caused by the independent noise on each aperture. The dominant noise source that was simulated was shot noise, in the form of a Gaussian distributed random variable, which had equal mean and variance. The errors increase for low signal levels. As the signal decreases from higher values the errors increase nearly linearly, on a log-log plot, until the signal decreases to about 1000 detected photoelectrons over a 256 x 256 pixel square detector or ~ 0.02 photoelectrons per pixel. At even lower signal the errors increase rapidly until the program registers the apertures randomly. Random registration errors imply that the signal could not be found over the noise.

The reason this system can operate at such low signal values is due to two separate sources of gain. For each aperture individually compression gain from using spatial heterodyne detection decreases the noise power allowing for lower signal levels to be processed. The noise will be uniformly distributed across the image plane at all spatial frequencies. However only a smaller image region is cropped and used to create the final image. The noise in the image is reduced by a factor of the cropped area divided by the total array area. [17]

The second source of gain is aperture gain after the sub-apertures are synthesized into a larger effective aperture. As described in Chapter 1, the resolution of the ladar systems is inversely proportional to the aperture diameter. Therefore the aperture gain is equal to the ratio of the synthetic aperture diameter over the diameter of a single sub-aperture. [1]

There are relatively small differences between the experimental and simulated results due to some effects that were neglected in the model. One such effect was extra scattered photons, primarily off of the CCD cover glass. If a few hundred extra photons were added to the simulation then the low signal sections of the plots would be aligned. Another effect was decreased mixing efficiency in the laboratory. Mixing efficiency is defined as the amount of the signal which mixes with the LO compared to the total signal hitting the CCD. If the mixing efficiency is not 100% then the model will be shifted to a lower signal level. In this case the model results were shifted by a factor of ~1.6.

For a standard ladar system the transmitted energy necessary to receive 1000 photoelectrons over the CCD reflected from a Lambertian target, can be calculated using Equation (43) [32]. Here the transmitted energy $E_{TX}$, is a function of the received energy $E_{RX}$, the range z, the target

reflectivity ρ, and the receiver aperture area $A_{RX}$. This equation assumes no atmospheric effects and that the target was larger than the area illuminated by the transmitter. As an example, consider a Lambertian target with 20% reflectivity at a range of 20 km from a receiver aperture with a diameter of 10 cm, neglecting atmospheric attenuation. The received energy in photoelectrons was converted to number of photons using a quantum efficiency of 70%. This signal was then converted to units of Joules using the energy per photon with a wavelength of 1.5 μm.

$$E_{TX} = \frac{\pi E_{RX} z^2}{\rho A_{RX}} \tag{43}$$

The transmitter energy necessary to generate 1000 photoelectrons over the receiver is 0.146 mJ. If 20,000 photoelectrons were desired the transmitter energy would have to be increased to 2.92 mJ. Of course if the atmosphere absorbs any of the radiation, more energy will be necessary. However this gives an idea of the levels of transmitted energy that would be needed to register overlapping apertures using this speckle cross-correlation process.

At low signals, registration errors were found to be less than 0.1 radians of piston phase and 0.1 waves of tilt over the aperture. If only two apertures are used to create a larger synthetic aperture, the image quality is not significantly affected by these small errors. However if the registration process adds small errors to each aperture in a larger synthetic aperture, then images appear out of focus. Larger synthetic apertures made up of 4, 6, 8 and 10 sub-apertures were created with compounded registration errors and the image quality suffered. The image quality was assessed using the MTF, and the effects were similar to those of defocus aberrations [20].

## 6.2 Future Work

This project demonstrated that even at low SNR for a shot noise limited coherent ladar system, a speckle cross-correlation algorithm can be used to accurately synthesize larger apertures. The future work will involve testing the limits of the assumptions made in this paper, such as determining the effect of atmospheric attenuation on these results. Another important factor is the size of the area that is cropped from the image plane. If a larger image area is cropped, then there will be more image information. It is expected that more image information would reduce the registration errors. However, that also means that more noise will be included in the cropped section, which could increase the errors. A smaller area can be cropped, which would reduce the amount of noise in the final image, but it would also remove some of the signal information.

Another project could investigate the registration errors at low SNR for other registration methods. For instance, many applications use image sharpness metrics to align the sub-apertures for sparse aperture arrays. An experiment similar to the one explained here, could be performed to find the effects of low signal levels on the accuracy of image sharpness algorithms. Other ladar systems use multiple registration steps in each plane to produce a more accurate synthetic aperture [8]. The influence of multi-plane registration on the MTF for low SNR situations could be determined by looking at whether the errors are reduced for each step. Characterizing the errors associated with the registration algorithm is very important for synthetic aperture ladar applications. This work demonstrated that even in photon starved conditions synthetic aperture ladar systems are very effective imaging systems particularly when speckle cross-correlation algorithms are used.

# REFERENCES


[1] D. J. Rabb, D. F. Jameson, J. W. Stafford, and A. J. Stokes. "*Multi-transmitter aperture synthesis.*" Optics Express. Vol. 18, No. 24, pp. 24937-24945 (2010).

[2] D. Rabb, D. Jameson, A. Stokes and J. Stafford. "*Distributed aperture synthesis.*" Optics Express. Vol. 18, No. 10, pp. 10334-10342 (2010).

[3] J. C. Marron, R. L. Kendrick. "*Distributed Aperture Active Imaging.*" Proc. of SPIE Vol. 6550, Laser Radar Technology and Applications XII, edited by M. D. Turner and G. W. Kamerman, paper 65500A (2007).

[4] N. J. Miller, M. P. Dierking, and B. D. Duncan. "*Optical sparse aperture imaging.*" Applied Optics. Vol. 46, No. 23, pp. 5933-5943 (2007).

[5] A. J. Stokes, B. D. Duncan, and M. P Dierking. "*Improving mid-frequency contrast in sparse aperture optical imaging systems based upon the Golay-9 array.*" Optics Express. Vol. 18, No. 5, pp. 4417-4427 (2010).

[6] J. E. Harvery, A. Kotha, and R. L. Phillips. "*Image characteristics in application utilizing dilute subaperture arrays.*" Applied Optics. Vol. 34, No. 16, pp. 2983-2992 (1995).

[7] R. Binet, J. Colinear, and J.-C. Lehureau. "*Short-range synthetic aperture imaging at 633 nm by digital holography.*" Applied Optics. Vol. 41, No. 23, pp. 4775-4782 (2002).

[8] S. M. Venable, B. D. Duncan, M. P. Dierking, and D. J. Rabb. "*Demonstrated resolution enhancement capability of a stripmap holographic aperture ladar system.*" Applied Optics. Vol. 51, No. 22, pp. 5531-5542 (2012).

[9] B. D. Duncan and M. P. Dierking. "*Holographic aperture ladar.*" Applied Optics. Vol. 48, No. 6, pp. 1168-1177 (2009).

[10] J. W. Stafford, B. D. Duncan, and M. P. Dierking. "*Experimental demonstration of a stripmap holographic aperture ladar system.*" Vol. 49, No. 12, pp. 2262-2270 (2010).

[11] S. M. Beck, J. R. Buck, W. F. Buell, R. P. Dickinson, D. A. Kozlowski, N. J. Marechal, and T. J. Wright. "*Synthetic-aperture imaging laser radar: laboratory demonstration and signal processing.*" Applied Optics. Vol. 44, No. 35, pp. 7621-7629 (2005).

[12] J.-C. Lehureau and J. Colineau. "*Optical Synthetic Aperture Imagery.*" Proc. of SPIE. Vol. 5816, Optical Pattern Recognition XVI, edited by D. P. Casasent and T.-H. Chao, pp. 54-65 (2005).

[13] T. J. Green, S. Marcus, and B. D. Colella. "*Synthetic-radar imaging with a solid-state laser.*" Applied Optics. Vol. 34, No. 30, pp. 6941-6949 (1995).

[14] T. G. Kyle. "*High resolution laser imaging system.*" Applied Optics. Vol. 28, No. 13, pp. 2651-2656 (1989).

[15] F. Le Clerc, M. Gross and L. Collot. "*Synthetic-aperture experiment in the visible with on-axis digital heterodyne holography.*" Optical Letters. Vol. 26, No. 20, pp. 1550-1552 (2001).

[16] A. E. Tippie and J. R. Fienup. "*Gigapixel Synthetic-Aperture Digital Holography: Sampling and Resolution Considerations.*" OSA Technical Digest: Imaging and Applied Optics (2011).

[17] A. E. Tippie and J. R. Fienup. "*Weak-Object Image Reconstructions with Single-Shot Digital Holography*." OSA Technical Digest: Biomedical Optics and 3D Imaging (2012).

[18] J. C. Marron and K. S. Schroeder. "*Holographic laser radar.*" Optics Letters. Vol. 18, No. 5, pp. 385-387 (1993).

[19] J. C. Marron. "*Photon Noise in Digital Holographic Detection.*" AFRL-RD-PS-TP-2009-1006. (2008).

[20] J. W. Goodman. Fourier Optics. 3rd Ed. Roberts & Co., Englewood, CO (2005).

[21] M. Guizar-Sicairos, S. T. Thurman and J. R. Fienup. "*Efficiency subpixel image registration algorithms.*" Optics Letters. Vol. 33, No. 2, pp. 156-158 (2008).

[22] M. Guizar. "*Efficient Subpixel Image Registration by Cross-Correlation.*" Matlab Central. MathWorks. Inc. (1994-2011). <http://www.mathworks.com/matlabcentral/fileexchange/18401-efficienct-subpixel-image-registration-by-cross-correlation>

[23] Redfern Integrated Optics, Inc. "RIO ORION Laser Module Product Brief." Santa Clara, CA (2012).

[24] Oz Optics. "Polarization Maintaining Fiber Patchcords and Connectors Manual." Ottawa, ON, Canada (2009).

[25] Oz Optics. "Miniature Inline Polarization Maintaining Splitters/Taps/Combiners Manual." Ottawa, ON, Canada (2005).

[26] Oz Optics. "Collimators and Focusers – Pigtail Style Manual." Ottawa, ON, Canada (2005).

[27] Agiltron, Inc. "CrystaLatch 1x2 Fiberoptic PM Swtich Manual." Woburn, MA (2011).

[28] Ophir Laser Measurement Group. "NOVA II: Laser Power/Energy Monitor User Manual." Ophir Optronics.

[29] FLIR. "SC2500 User Manual." North Billerica, MA.

[30] J. W. Goodman. Speckle Phenomena in Optics. Roberts & Co., Englewood, CO (2007).

[31] J. R. Taylor. An Introduction to Error Analysis: The Study of Uncertainties in Physical Measurements. 2nd Ed. University Science Books, Sausalito, CA (1997).

[32] R. D. Richmond and S. C. Cain. Direct-Detection LADAR Systems. SPIE Press, Bellingham, WA (2010).

# APPENDIX A: SIMULATION IN MATLAB

```
% This program investigates the registration errors from the
% dftups_1000 program as a function of signal level. A white target
% with circularly complex Gaussian speckle noise mixes with an LO and
% is captured on two overlapping apertures. The apertures are NOT
% shifted therefore the overlap region is the full aperture size.
% Independent shot noise is added to each aperture. Only the
% overlapping regions are processed (holographically) and fed to the
% registration program and the output row, column and phase shifts
% required to align the apertures will be recorded, averaged and
% plotted.

clear all;

close all;

clc;

%%%%%%%%%%%%%%%%%%%%%%%%%%%%%%%%%%%%%%%%%%%%%%%%%%%%%%%%%%%%%%%%%%%%%%%%%%%%%%%
%%%%%%%%%% This section initiates parameters %%%%%%%%%%%%%%%%%%%%
%%%%%%%%%%%%%%%%%%%%%%%%%%%%%%%%%%%%%%%%%%%%%%%%%%%%%%%%%%%%%%%%%%%%%%%%%%%%%%%

% Number of trials with independent speckle realizations:
Naverages = 1280;

% Wavelength in meters:
lambda = 1545.0e-9;

% Range to the target in meters:
z = 2.0;

% Number of pixels across one dimension of receiver (RX):
N = 256;

% Pixel pitch or pixel size, in meters:
Px = 30e-6;

% RX aperture diameter in meters:
Dap = N*Px;

% Target diameter in meters:
Dobj = 20e-3;

% Propagation induced pupil plane pixel size, in meters:
pp = (lambda*z)/Dobj;

% Number of speckles seen by the RX
Nspeckle = round(Dap/pp);

% Beam radius of the transmitter (TX) spot size at the target, in
% meters:
w = 9.8e-3;
```

```
% Target plane coordinates:
x = [-128:127]*(lambda*z/Dap);
[xTP yTP] = meshgrid(x,x);

% Number of signal photons over the RX
Nphotons = [9.82, 19.54, 48.58, 101.18, 151.03, 196.44, 295.72, 391.83,
   485.82, 585.10, 987.49, 1478.59, 1969.69, 2978.30, 4900.47, 7403.51,
   9927.68, 19749.74, 49110.33, 98748.72];

% Number of pixels in the overlap, in this case the entire CCD
NpixINoverlap = N*N;

%%%%%%%%%%%%%%%%%%%%%%%%%%%%%%%%%%%%%%%%%%%%%%%%%%%%%%%%%%%%%%%%%%%%%%%%%%%%
%%%%%%%%%%%%%%%%%%%% Simulating the LO %%%%%%%%%%%%%%%%%%%%%%%%
%%%%%%%%%%%%%%%%%%%%%%%%%%%%%%%%%%%%%%%%%%%%%%%%%%%%%%%%%%%%%%%%%%%%%%%%%%%%

% Full well capacity of the FLIR SC2500 camera
full_well_cap = 0.17*10^6;

% Half well capacity of the FLIR SC2500 camera
half_well_cap = full_well_cap/2;

% Quantum efficiency of the FLIR SC2500 camera
quantum_eff = 0.7;

% Attenuation factor due to integrating over square pixels, instead of %
taking max
MTF_atten = sinc(0.25)*sinc(0.25);

% Pupil Plane coordinates:
n = linspace(-(Dap/2), (Dap/2), N);
[xPP yPP] = meshgrid(n);

% Beam radius of the LO spot size at the RX, in meters:
wLO = 9.8e-3;

% Amplitude of the LO, in units of square root of photons
ALO = sqrt(half_well_cap/quantum_eff);

% Gaussian intensity mask for the LO:
LOmask = exp(-(xPP.^2+yPP.^2)/wLO.^2);
LOmask = LOmask.*(ALO/mean2(LOmask));

% Tilted plane wave phase of the LO
PhaseLO = 2*pi.*(N/Dap)*(-xPP/4+yPP/4);

% LO tilted plane wave with half well capacity amplitude:
LO = LOmask.*exp(1j*PhaseLO);

%%%%%%%%%%%%%%%%%%%%%%%%%%%%%%%%%%%%%%%%%%%%%%%%%%%%%%%%%%%%%%%%%%%%%%%%%%%%
%%%%%%%%%%%%%%%%%%%% Initialize Variables %%%%%%%%%%%%%%%%%%%%%%%%
%%%%%%%%%%%%%%%%%%%%%%%%%%%%%%%%%%%%%%%%%%%%%%%%%%%%%%%%%%%%%%%%%%%%%%%%%%%%

% Initialize Registration Piston Phase Shift:
```

```
shift_p = zeros(1,Naverages);

% Initialize Registration Row Shift:
shift_r = zeros(1,Naverages);

% Initialize Registration Column Shift:
shift_c = zeros(1,Naverages);

% Initialize RMS Registration Piston Phase Shift:
shift_p_rms = zeros(1,length(Nphotons));

% Initialize RMS Registration Row Shift:
shift_r_rms = zeros(1,length(Nphotons));

% Initialize RMS Registration Column Shift:
shift_c_rms = zeros(1,length(Nphotons));

%%%%%%%%%%%%%%%%%%%%%%%%%%%%%%%%%%%%%%%%%%%%%%%%%%%%%%%%%%%%%%%%%%%%%%%%%%%%
%%%%%% Loop through various Signal Levels and Trials %%%%%%%%%%%%
%%%%%%%%%%%%%%%%%%%%%%%%%%%%%%%%%%%%%%%%%%%%%%%%%%%%%%%%%%%%%%%%%%%%%%%%%%%%

% Loop through various signal levels:
for jj = 1: length(Nphotons);

    % Loop through 1280 trials:
    for kk = 1:Naverages;


      %%%%%%%%%%%%%%%%%%%%%%%%%%%%%%%%%%%%%%%%%%%%%%%%%%%%%%%%%%%%%%%%%%%%%%%%%%%%
      %%%%%%%%%%%%%% Create Target and Signal %%%%%%%%%%%%%%%%%%%
      %%%%%%%%%%%%%%%%%%%%%%%%%%%%%%%%%%%%%%%%%%%%%%%%%%%%%%%%%%%%%%%%%%%%%%%%%%%%

        % Circularly Gaussian Random Target (in Target plane):
        target = randn(N)+1j*randn(N);

        % Gaussian intensity mask of the TX (in Target plane):
        mask = exp(-(xTP.^2+yTP.^2)/w.^2);

        % Reflected signal (in Target plane):
        Reflect_Signal = target.*mask;

        % Signal propagated to the Pupil Plane:
        pupil = ft2(Reflect_Signal);

        % Adjusted the Signal Amplitude to the desired number of
        % photons in the overlap region (in Pupil Plane):
        Signal = pupil.*sqrt(Nphotons(jj)/ ...
                  (mean2(abs(pupil).^2)*NpixINoverlap));

      %%%%%%%%%%%%%%%%%%%%%%%%%%%%%%%%%%%%%%%%%%%%%%%%%%%%%%%%%%%%%%%%%%%%%%%%%%%%
      %%%%%%%%%%%%%%%% Mix Signal and LO %%%%%%%%%%%%%%%%%%%%%%%
      %%%%%%%%%%%%%%%%%%%%%%%%%%%%%%%%%%%%%%%%%%%%%%%%%%%%%%%%%%%%%%%%%%%%%%%%%%%%

        % Interference Intensity Fringe Pattern (in Pupil Plane):
```

```
  fringes = quantum_eff*(abs(Signal).^2 + abs(LO).^2 + ...
             MTF_atten*(conj(LO).*Signal + LO.*conj(Signal)));

%%%%%%%%%%%%%%%%%%%%%%%%%%%%%%%%%%%%%%%%%%%%%%%%%%%%%%%%%%%%%%%%%%%%%%%%%%%%
%%%%% Create Two Apertures with Independent Noise %%%%%%%%%
%%%%%%%%%%%%%%%%%%%%%%%%%%%%%%%%%%%%%%%%%%%%%%%%%%%%%%%%%%%%%%%%%%%%%%%%%%%%

  % First aperture produced by adding independent Shot and
  % Detector noise to the intensity pattern (in Pupil Plane):
  ap1_Noise = fringes + sqrt(fringes).*randn(size(fringes)) + ...
            150*randn(size(fringes));

  % Second aperture produced by adding independent Shot and
  % Detector noise to the intensity pattern (in Pupil Plane):
  ap2_Noise = fringes + sqrt(fringes).*randn(size(fringes)) + ...
            150*randn(size(fringes));

  % Simulated DC and detected background noise, in units of
  % digital counts:
  DC = quantum_eff*((abs(LO)).^2).*(2^14/full_well_cap);

  % First aperture in recorded digital counts with the DC
  % subtracted:
  ap1_Noise = round((ap1_Noise).*(2^14/full_well_cap)) - DC;

  % Second aperture in recorded digital counts with the DC
  % subtracted:
  ap2_Noise = round((ap2_Noise).*(2^14/full_well_cap)) - DC;

%%%%%%%%%%%%%%%%%%%%%%%%%%%%%%%%%%%%%%%%%%%%%%%%%%%%%%%%%%%%%%%%%%%%%%%%%%%%
%%%%%%%%%%%%% IFT to Image Plane %%%%%%%%%%%%%%%%%%%%%%%%
%%%%%%%%%%%%%%%%%%%%%%%%%%%%%%%%%%%%%%%%%%%%%%%%%%%%%%%%%%%%%%%%%%%%%%%%%%%%

  % First image propagated to the Image Plane:
  im1 = ift2(ap1_Noise);

  % Second image propagated to the Image Plane:
  im2 = ift2(ap2_Noise);



%%%%%%%%%%%%%%%%%%%%%%%%%%%%%%%%%%%%%%%%%%%%%%%%%%%%%%%%%%%%%%%%%%%%%%%%%%%%
%%%%%%%%%% Crop out the real Image Component %%%%%%%%%%%%%
%%%%%%%%%%%%%%%%%%%%%%%%%%%%%%%%%%%%%%%%%%%%%%%%%%%%%%%%%%%%%%%%%%%%%%%%%%%%

  % First image cropped from lower left quadrant (in Image
  % Plane):
  im1_crop = im1(153:232,25:104);

  % Second image cropped from lower left quadrant (in Image
  % Plane):
  im2_crop = im2(153:232,25:104);

%%%%%%%%%%%%%%%%%%%%%%%%%%%%%%%%%%%%%%%%%%%%%%%%%%%%%%%%%%%%%%%%%%%%%%%%%%%%
%%%%%%%%%%%%% FT Back to Pupil Plane %%%%%%%%%%%%%%%%%%%%
```

```
        %%%%%%%%%%%%%%%%%%%%%%%%%%%%%%%%%%%%%%%%%%%%%%%%%%%%%%%%%%%%%%%%%%%%%%%

          % Propagate the images to the Pupil Plane and place the two
          % apertures in a single 3D array according to their relative
          % postions. Here it has been estimated that the apertures are
          % perfectly aligned.
          [m n] = size(im1_crop);
          padppl = zeros(m,n,2);
          padppl(:,:,1) = ft2(im1_crop);
          padppl(:,:,2) = ft2(im2_crop);

        %%%%%%%%%%%%%%%%%%%%%%%%%%%%%%%%%%%%%%%%%%%%%%%%%%%%%%%%%%%%%%%%%%%%%%%
        %%%%%%%%%%%%%%%%%%%% Registration %%%%%%%%%%%%%%%%%%%%%%%%
        %%%%%%%%%%%%%%%%%%%%%%%%%%%%%%%%%%%%%%%%%%%%%%%%%%%%%%%%%%%%%%%%%%%%%%%

          % Plug the pupil plane information into the registration
          % program. Aperture 1 is the reference which Aperture 2 will be
          % aligned to.
          [output] = dftups_1000(padppl(:,:,1),padppl(:,:,2));

          % Record the registration algorithm output values:
          % Registration Piston Phase Shift:
          shift_p(kk) = output(1);

          % Registration Row Shift:
          shift_r(kk) = output(2);

          % Registration Column Shift:
          shift_c(kk) = output(3);

      end

      % RMS Piston Phase Errors for 1280 trials at a specific signal
      % level:
      shift_p_rms(jj) = sqrt(mean(shift_p.^2));

      % RMS Row Tilt Errors for 1280 trials at a specific signal level:
      shift_r_rms(jj) = sqrt(mean(shift_r.^2));



      % RMS Column Tilt Errors for 1280 trials at a specific signal
      % level:
      shift_c_rms(jj) = sqrt(mean(shift_c.^2));

end

% Plot the Registration Errors as a function of Signal Level:
figure(1); loglog(Nphotons, shift_p_rms, 'go-');
      title('Log Log RMS Piston Phase Shifts');
      xlabel('log # photons in overlap region');
      ylabel('Log RMS Piston Phase Shifts [radians]');
      ylim([10^-4 10^1]);

figure(2); loglog(Nphotons, shift_r_rms,'bo-', Nphotons, ...
```

```
shift_c_rms,'ro-');
title('LogLog RMS Row and Column Shifts');
xlabel('log # photons in overlap region');
ylabel('Log RMS Row and Column Shifts [waves]');
ylim([10^-4 10^1]);
```

# APPENDIX B: DATA PROCESSING IN MATLAB

```
% This program processes the laboratory data. Adjacent frames will be
% registered to find the piston phase and tilt errors as a function of
% signal level.

clear all;
close all;
clc;

%%%%%%%%%%%%%%%%%%%%%%%%%%%%%%%%%%%%%%%%%%%%%%%%%%%%%%%%%%%%%%%%%%%%%%%%%%%%%%%
%%%%%%%%%% This section initiates parameters %%%%%%%%%%%%%%%%%%%
%%%%%%%%%%%%%%%%%%%%%%%%%%%%%%%%%%%%%%%%%%%%%%%%%%%%%%%%%%%%%%%%%%%%%%%%%%%%%%%

% Number of frames captured for each signal level at a single location.
Nframes = 128;

% Number of trials, 10 trials with 128 frames each for a total of 1280 %
images.
Ntrials = 10;

% wavelength in meters
lambda = 1545.0e-9;

% range in meters
z = 2.0;

% Number of pixels across one dimension of the receiver (RX)
N = 256;

% Pixel pitch or pixel size in meters
Px = 30e-6;

% RX aperture diameter in meters
Dap = N*Px;

% Target diameter in meters
Dobj = 20e-3;

% Propagation induced pupil plane pixel size in meters
pp = (lambda*z)/Dobj;

% Number of Speckles seen by the RX
Nspeckle = round(Dap/pp);

% Number of Signal photons over the RX
Nphotons = [10.24, 19.89, 49.45, 102.98, 153.71, 199.93, 300.98,
      398.79, 494.46, 595.50, 1005.04, 1504.88, 2004.71, 3031.25,
      4987.59, 7535.13, 10104.17, 20100.85, 49983.40, 100504.25];

% Number of pixels in the overlap region, in this case the entire CCD.
NpixINoverlap = N*N;
```

```
%%%%%%%%%%%%%%%%%%%%%%%%%%%%%%%%%%%%%%%%%%%%%%%%%%%%%%%%%%%%%%%%%%%%%%%%%%%%
%%%%%%%%%%%%%%%%%%%% Initialize Variables %%%%%%%%%%%%%%%%%%%%
%%%%%%%%%%%%%%%%%%%%%%%%%%%%%%%%%%%%%%%%%%%%%%%%%%%%%%%%%%%%%%%%%%%%%%%%%%%%

% Initialize fringe data array:
fringes_data = zeros(N,N,Nframes,Ntrials);

% Initialize fringe data with the static background noise subtracted:
fringesNoDC = zeros(Nframes,N*N);

% Initialize Registration Phase Shift:
shift_p = zeros(Ntrials,Nframes);

% Initialize Registration Row Shift:
shift_r = zeros(Ntrials,Nframes);

% Initialize Registration Column Shift:
shift_c = zeros(Ntrials,Nframes);

% Initialize RMS Registration Piston Phase Shift:
shift_p_rms = zeros(1,length(Nphotons));

% Initialize RMS Registration Row Shift:
shift_r_rms = zeros(1,length(Nphotons));

% Initialize RMS Registration Column Shift:
shift_c_rms = zeros(1,length(Nphotons));

% Initialize average LO only value for each pixel over 128 frames.
LOavg2D = zeros(Ntrials,length(Nphotons));

%%%%%%%%%%%%%%%%%%%%%%%%%%%%%%%%%%%%%%%%%%%%%%%%%%%%%%%%%%%%%%%%%%%%%%%%%%%%
%%%%%% Loop through various Signal Levels and Trials %%%%%%%%%%%
%%%%%%%%%%%%%%%%%%%%%%%%%%%%%%%%%%%%%%%%%%%%%%%%%%%%%%%%%%%%%%%%%%%%%%%%%%%%

% Loop through various signal levels:
for jj = 1: length(Nphotons);

        % Loop through 10 trials:
    for kk = 1:Ntrials;

      %%%%%%%%%%%%%%%%%%%%%%%%%%%%%%%%%%%%%%%%%%%%%%%%%%%%%%%%%%%%%%%%%%%%%%%%
  %%%%%%%%% Load the data captured in the laboratory %%%%%%%%%%%
      %%%%%%%%%%%%%%%%%%%%%%%%%%%%%%%%%%%%%%%%%%%%%%%%%%%%%%%%%%%%%%%%%%%%%%%%

        % Load 128 Signal + LO frames for a given signal and trial
        % This is an array where each row has the intensity value for
        % each pixel.
        load(['Inten',num2str(jj),num2str(kk)],'a');
        fringes_raw = a;

        % Load 128 LO only frames for a given signal and trial
        % This is an array where each row has the intensity value for
        % each pixel.
```

```
    load(['IntenLO',num2str(jj),num2str(kk)],'a');
    LO_raw = a;

    % Average value of the LO at each pixel for 128 frames
    LOavg = mean(LO_raw);

    % Loop through 128 frames for each trial:
    for ll = 1:Nframes;

        % Subtract Average LO at each pixel from the Signal + LO
        % data:
        fringesNoDC(ll,:) = fringes_raw(ll,:) - LOavg;

        % Reshape the Signal data into a 3D array of 256 x 256 x
        % 128:
        fringes_data(:,:,ll,kk) =
                          (reshape(fringesNoDC(ll,:),256,256)).';

    end

end

  %%%%%%%%%%%%%%%%%%%%%%%%%%%%%%%%%%%%%%%%%%%%%%%%%%%%%%%%%%%%%%%%%%%%%%%%%%%%
  %%%%%%%%%% Register the Adjacent Frames %%%%%%%%%%%%%%%%%%
  %%%%%%%%%%%%%%%%%%%%%%%%%%%%%%%%%%%%%%%%%%%%%%%%%%%%%%%%%%%%%%%%%%%%%%%%%%%%

% Loop through 10 trials:
for kk = 1:Ntrials;

    % Loop through 128 frames for each trial:
    for ll = 1:Nframes-1;

        % Set the two apertures to be registered as adjacent frame
        % data
        ap1 = fringes_data(:,:,ll,kk);
        ap2 = fringes_data(:,:,ll+1,kk);



  %%%%%%%%%%%%%%%%%%%%%%%%%%%%%%%%%%%%%%%%%%%%%%%%%%%%%%%%%%%%%%%%%%%%%%%%%%%%
  %%%%%%%%%%%%%% IFT to Image Plane %%%%%%%%%%%%%%%%%%%%%%%%
  %%%%%%%%%%%%%%%%%%%%%%%%%%%%%%%%%%%%%%%%%%%%%%%%%%%%%%%%%%%%%%%%%%%%%%%%%%%%

        % Propagate each aperture to the Image Plane:
        im1 = ift2(ap1);
        im2 = ift2(ap2);

  %%%%%%%%%%%%%%%%%%%%%%%%%%%%%%%%%%%%%%%%%%%%%%%%%%%%%%%%%%%%%%%%%%%%%%%%%%%%
  %%%%%%%%%% Crop out the real Image Component %%%%%%%%%%%%%%
  %%%%%%%%%%%%%%%%%%%%%%%%%%%%%%%%%%%%%%%%%%%%%%%%%%%%%%%%%%%%%%%%%%%%%%%%%%%%

        % Crop out the real image component in the lower left
        % quadrant:
        im1_crop = im1(153:232,25:104);
```

```
            im2_crop = im2(153:232,25:104);

        %%%%%%%%%%%%%%%%%%%%%%%%%%%%%%%%%%%%%%%%%%%%%%%%%%%%%%%%%%%%%%%%%%%%%%%%
        %%%%%%%%%%%%%% FT Back to Pupil Plane %%%%%%%%%%%%%%%%%%%%
        %%%%%%%%%%%%%%%%%%%%%%%%%%%%%%%%%%%%%%%%%%%%%%%%%%%%%%%%%%%%%%%%%%%%%%%%

            % Propagate each image back to the Pupil Plane, and place
            % both apertures into a 3D array according to their
            % relative postions. Here it has been estimated that the
            % apertures are perfectly aligned.
            [m n] = size(im1_crop);
            padppl = zeros(m,n,2);
            padppl(:,:,1) = ft2(im1_crop);
            padppl(:,:,2) = ft2(im2_crop);

        %%%%%%%%%%%%%%%%%%%%%%%%%%%%%%%%%%%%%%%%%%%%%%%%%%%%%%%%%%%%%%%%%%%%%%%%
        %%%%%%%%%%%%%%%%%%% Registration %%%%%%%%%%%%%%%%%%%%%%%
        %%%%%%%%%%%%%%%%%%%%%%%%%%%%%%%%%%%%%%%%%%%%%%%%%%%%%%%%%%%%%%%%%%%%%%%%

            % Plug the pupil plane information into the registration
            % program. Aperture 1 is the reference which Aperture 2
            % will be aligned to.
            [output] = dftups_1000(padppl(:,:,1),padppl(:,:,2));

            % Record the registration algorithm output values:
            % Registration Piston Phase Shift:
            shift_p(kk,ll) = output(1);

            % Registration Row Shift:
            shift_r(kk,ll) = output(2);

            % Registration Column Shift:
            shift_c(kk,ll) = output(3);

        end

    end



    % RMS Piston Phase Errors for 1280 total frames at each signal
    % level:
    shift_p_rms(jj) = sqrt(mean2(shift_p.^2));

    % RMS Row Tilt Errors for 1280 total frames at each signal level:
    shift_r_rms(jj) = sqrt(mean2(shift_r.^2));

    % RMS Column Tilt Errors for 1280 total frames at each signal
    % level:
    shift_c_rms(jj) = sqrt(mean2(shift_c.^2));

end

% Plot the Registration Errors as a function of Signal Level:
```

```
figure(1); loglog(Nphotons, shift_p_rms, 'go-');
      title('LogLog RMS Piston Phase Shifts');
      xlabel('log # photons in overlap region');
      ylabel('Log RMS Piston Phase Shifts [radians]');
      ylim([10^-4 10^1]);

figure(2); loglog(Nphotons, shift_r_rms,'bo-', Nphotons, ...
      shift_c_rms,'ro-');
      title('LogLog RMS Row and Column Shifts');
      xlabel('log # photons in overlap region');
      ylabel('Log RMS Row and Column Shifts [waves]');
ylim([10^-4 10^1]);
```

# APPENDIX C: MTF CALCULATION IN MATLAB

```
% This program investigates the effect of given piston phase errors as
% well as tip and tilt errors on the MTF of a synthetic aperture. These
% effects will be investigated at high signal levels only. The
% apertures will not be registered together, they will simply be
% combined. Also the object being viewed is a point target so we can
% get all the MTF information from one target.

clear all;

close all;

clc;

% Number of times each independent speckle and noise realization is
% found and registered, these will be averaged together to get one
% number for each signal level
Naverage = 100;

% Number of sub-apertures in a given synthetic aperture
Naperture = [2, 4, 6, 8, 10];

% wavelength in meters
lambda = 1545.0e-9;

% range in meters
z = 2.0;

% Number of pixels across one dimension of the receiver (RX)
N = 256;

% Pixel pitch or pixel size in meters
Px = 30e-6;

% RX aperture diameter in meters
Dap = N*Px;

% Target diameter in meters
Dobj = 20e-3;

% Propagation induced pupil plane pixel size in meters
pp = (lambda*z)/Dobj;

% Number of speckles seen by a single sub-aperture
Nspeckle = round(Dap/pp);

% Diameter of the final synthetic aperture (each sub-aperture overlaps
% by half an aperture diameter) in meters
Dsyn = Dap*((Naperture + 1)/2);

% Loop through all the synthetic aperture sizes and calculate the
% number of speckles across the synthetic aperture:
for k = 1:length(Naperture);
```

```
        if floor(Naperture(k)/2) == (Naperture(k)/2)

            Nsynap(k) = ((Naperture(k)/2)+0.5)*Nspeckle + 1;

        else

            Nsynap(k) = ((Naperture(k)/2)+0.5)*Nspeckle;

        end

end

% Amount of aperture overlap in the x direction (rows)
overlapX = Dap;

% Amount of aperture overlap in the y direction (columns)
overlapY = 0.5*Dap;

% Registration Coefficients chosen using experimental results
% Piston error [radians]
p = 0.1445;

% Row shift error [pixels] or [waves of tilt over half an aperture]
r = 0.1045;

% Column shift error [pixels] or [waves of tilt over half an aperture]
c = 0.0877;

%Initial tip/tilt/piston on the first aperture
p1 = 0;
r1 = 0;
c1 = 0;

% Pupil Plane coordinates:
n = (-24.5:1:24.5)./25;
[x y] = meshgrid(n);

% Initialize the synthetic aperture MTF. It needs to be large enough
% for each synthetic aperture size to plotted on the same scale.
b = Nsynap(length(Naperture));
MTF_syn = zeros(1,b,length(Naperture));

% Loop through the different synthetic aperture sizes:
for kk = 1:length(Naperture);

    % Initialize the array of sub-apertures:
    ap = zeros(Nspeckle,Nsynap(kk),Naperture(kk));

    % Create the first sub-aperture as a uniform array.
    ap(:,1:50,1) = ones(Nspeckle);

    % Initialize the variables used to arrange each sub-aperture
    % relative to the others.
    start = zeros(1, Naperture(kk));
```

```
last = zeros(1, Naperture(kk));

% Initialize an array for the average MTF over 100 trials
MTF_avg = zeros(1,2*Nsynap(kk));

% Initialize an array for the MTF for each trial
MTF = zeros(1,2*Nsynap(kk),Naverage);

% Loop through 100 trials for each synthetic aperture length
for ii = 1:Naverage;

    % Initialize an array for each relative registration error
    % Relative Piston Phase applied to sub-aperture n
    pn = zeros(1, Naperture(kk));

    % Relative Row Tilt applied to sub-aperture n
    rn = zeros(1, Naperture(kk));

    % Relative Column Tilt applied to sub-aperture n
    cn = zeros(1, Naperture(kk));

    % Difference between relative piston phase for apertures n and
    % m, set as a normally distributed random number between 0 & 1,
    % that is weighted by the experimental results.
    pnm = p.*randn(1, Naperture(kk)-1);

    % Difference between relative row tilt for apertures n and m,
    % set as a normally distributed random number between 0 & 1,
    % that is weighted by the experimental results.
    rnm = r.*randn(1, Naperture(kk)-1);

    % Difference between relative column tilt for apertures n and
    % m, set as a normally distributed random number between 0 & 1,
    % that is weighted by the experimental results.
    cnm = c.*randn(1, Naperture(kk)-1);

    % Loop through each sub-aperture:
    for jj = 2:Naperture(kk);

        % Set the initial registration errors to start at zero.
        pn(jj) = p1;
        rn(jj) = r1;
        cn(jj) = c1;

        % For the second sub-apertures,calculate the relative
        % piston phase:
        if jj ==2;

            pn(jj) = pn(jj-1) + pnm(jj-1) + pi*cnm(jj-1);

        % For all of the other sub-apertures, calculate the
        % relative piston phase:
        else
```

```
            pn(jj) = pn(jj-1) + pi*cnm(jj-2) + pnm(jj-1) +...
                          pi*cnm(jj-1);

        end

        % Relative Row Shift:
        rn(jj) = rn(jj)+rnm(jj-1);

        % Relative Column shift:
        cn(jj) = cn(jj)+cnm(jj-1);

        % Starting and Ending locations for each sub-aperture
        start(jj) = (jj-1)*(Nspeckle/2)+1;

        last(jj) = start(jj)+Nspeckle-1;

        % Create each sub-aperture with the relative piston and
        % tilt errors.
        ap(:,start(jj):last(jj),jj) =
                          ones(Nspeckle).*exp(1j*(pn(jj)+ ...
                                pi*((Dap/overlapX)*rn(jj)*x + ...
                                      (Dap/overlapY)*cn(jj)*y)));

    end

    % Combine all of the sub-apertures into a synthetic aperture:
    combine = sum(ap,3);

    % Adjust the amplitude in the overlapping sections to avoid
    % double counting:
    combine(:, start(2):Nsynap(kk)-(Nspeckle/2)-1) =
              combine(:, start(2):Nsynap(kk)-(Nspeckle/2)-1)*0.5;

    % Embed the synthetic aperture in an array of zeros that is
    % twice as large in both dimensions
    [m n] = size(combine);
    combine_padded = padarray(combine, [(2*m-m)/2 (2*n-n)/2]);

    % FT the synthetic aperture to the focal plane. The zero-
    % padding effectively upsamples each point by a factor of 2.
    focal = ft2(combine_padded);

    % Take the modulus squared to find the Intensity Point Spread
    % Function:
    PSF = (abs(focal)).^2;

    % FT to calculate the Spatial Frequency Content:
    SFC = ft2(PSF);

    % The MTF is the normalized central line of the Spatial
    % Frequency Content:
    MTF(:,:,ii) = abs(SFC(Nspeckle+1,:))./max(max(abs(SFC)));

end
```

```
    % Average the MTF over 100 trials for each synthetic aperture:
    MTF_avg = mean(MTF,3);

    % Crop out only the positive spatial frequencies:
    w = length(MTF_avg);
    MTF_syn(:,1:(w/2),kk) = MTF_avg(:,(w/2)+1:w);

end

% Bandwidth as a function of synthetic aperture diameter:
syn_mtf_cutoff = Dsyn/(lambda*z*1000);

% Initiate variables to determine the theoretical MTF:
a = length(MTF);
X = zeros(length(Naperture),a/2);
theoretical = zeros(length(Naperture),a/2);

% Loop through each synthetic aperture size:
for ll = 1:length(Naperture);

    % The spatial frequency coordinates:
    X(ll,:) = [0:(a/2)-1].*(syn_mtf_cutoff(ll)/((a/2)-1));

    % Theoretical MTF for each synthetic aperture:
    theoretical(ll,:) = 1 - (X(ll,:)/syn_mtf_cutoff(ll));

end

% Plot the average simulated MTF for each synthetic aperture
figure(1); plot(X(5,:),MTF_syn(:,:,1),'r-',X(5,:),MTF_syn(:,:,2),'b-
            ',X(5,:),MTF_syn(:,:,3),'c-',X(5,:),MTF_syn(:,:,4),'m-
            ',X(5,:),MTF_syn(:,:,5),'g-');
            xlabel('Spatial Frequency [cyc/mm]');
            ylabel('MTF'); legend('2','4','6','8','10');
            title('Synthetic Aperture MTF as Function of Number of Sub-
                  Apertures');

% Plot the average MTF and the theoretical MTF for each synthetic
% aperture
figure(2); plot(X(1,:),theoretical(1,:),'k-',X(5,:),MTF_syn(:,:,1),'k—
            ');
            title('MTF for Synthetic Aperture with 2 Apertures');
            xlabel('Spatial Frequency [cyc/mm]'); ylabel('MTF');
            legend('Theoretical without errors','Simulated with
                        errors');
figure(3); plot(X(2,:),theoretical(2,:),'k-',X(5,:),MTF_syn(:,:,2),'k—
            ');
            title('MTF for Synthetic Aperture with 4 Apertures');
            xlabel('Spatial Frequency [cyc/mm]'); ylabel('MTF');
            legend('Theoretical without errors','Simulated with
                        errors');
figure(4); plot(X(3,:),theoretical(3,:),'k-',X(5,:),MTF_syn(:,:,3),'k—
            ');
            title('MTF for Synthetic Aperture with 6 Apertures');
```

```
            xlabel('Spatial Frequency [cyc/mm]'); ylabel('MTF');
            legend('Theoretical without errors','Simulated with
                        errors');
figure(5); plot(X(4,:),theoretical(4,:),'k-',X(5,:),MTF_syn(:,:,4),'k—
            ');
            title('MTF for Synthetic Aperture with 8 Apertures');
            xlabel('Spatial Frequency [cyc/mm]'); ylabel('MTF');
            legend('Theoretical without errors','Simulated with
                        errors');
figure(6); plot(X(5,:),theoretical(5,:),'k-',X(5,:),MTF_syn(:,:,5),'k—
            ');
            title('MTF for Synthetic Aperture with 10 Apertures');
            xlabel('Spatial Frequency [cyc/mm]'); ylabel('MTF');
            legend('Theoretical without errors','Simulated with
                        errors');
```

# LIST OF SYMBOLS, ABBREVIATIONS, AND ACRONYMS

| ACRONYM | DESCRIPTION |
|---|---|
| AFRL | Air Force Research Laboratory |
| CCD | Charge Coupled Device |
| DFT | Discrete Fourier Transform |
| FPA | Focal Plane Array |
| LO | Local Oscillator |
| MTF | Modulation Transfer Function |
| PM | Polarization Maintaining |
| QE | Quantum Efficiency |
| RMS | Root Mean Square |
| SAR | Synthetic Aperture Radar |
| SAL | Synthetic Aperture Ladar |
| SNR | Signal to Noise Ratio |
| **SYMBOL** | **DESCRIPTION** |
| TX | Transmitter |
| RX | Receiver |
| $\mathcal{FT}^{-1}\{\}$ | Inverse Fourier Transform |
| $\mathcal{FT}\{\}$ | Inverse Fourier Transform |
| $()^*$ | Complex conjugate |
| $\circledast$ | Convolution |
| f | Target field at object |
| g | LO field at object (point source) |
| F | Fourier transform of f |
| G | Fourier transform of g |
| I | Irradiance recorded by receiver |
| x,y | Target plane coordinates |
| $\xi$, $\eta$ | Pupil plane coordinates |
| z | Distance along optical axis |
| $\phi$ | Phase offset |
| $\tau$ | Integration time |
| $\lambda$ | Optical wavelength |

| SYMBOL | DESCRIPTION |
|---|---|
| $\rho$ | Target Reflectivity |
| h | Planck's constant |
| k | Boltzmann's constant |
| $E_{TX}$, $E_{RX}$ | Energy transmitted and received |
| $A_{RX}$ | Area of receiver |
| T | Temperature |
| B | Bandwidth |
| P | Power |
| $\nu$ | Frequency of light |
| $P_B$ | Background noise |
| $\mu$ | Average value |
| $\sigma$ | Standard deviation |
| $< >$ | Expected value |